Liquid-Phase Transmission Electron Microscopy for Studying Colloidal Inorganic Nanoparticles

Byung Hyo Kim, Jiwoong Yang, Donghoon Lee, Back Kyu Choi, Taeghwan Hyeon, and Jungwon Park*

For the past few decades, nanoparticles of various sizes, shapes, and compositions have been synthesized and utilized in many different applications. However, due to a lack of analytical tools that can characterize structural changes at the nanoscale level, many of their growth and transformation processes are not yet well understood. The recently developed technique of liquid-phase transmission electron microscopy (TEM) has gained much attention as a new tool to directly observe chemical reactions that occur in solution. Due to its high spatial and temporal resolution, this technique is widely employed to reveal fundamental mechanisms of nanoparticle growth and transformation. Here, the technical developments for liquid-phase TEM together with their application to the study of solution-phase nanoparticle chemistry are summarized. Two types of liquid cells that can be used in the high-vacuum conditions required by TEM are discussed, followed by recent in situ TEM studies of chemical reactions of colloidal nanoparticles. New findings on the growth mechanism, transformation, and motion of nanoparticles are subsequently discussed in detail.

1. Introduction

Many important reactions in chemistry, physics, and biology occur in solution. Imaging of subjects in a liquid media is in high demand for gaining a better understanding of these reactions at the atomic and molecular levels. Liquid-phase transmission electron microscopy (TEM) is an emerging technology that provides new opportunities for direct and real-time visualization of dynamic processes in solution.[1–5] In the early history of TEM development, one of the pioneering studies was a TEM study of the ultrastructures of wet biological specimens embedded between thin aluminum foils.[6] However, further development of liquid-phase TEM to exploit high spatial resolution for the study of liquid-phase dynamics has been limited. Moreover, this was regarded as a daunting goal until the recent advance of microfabrication techniques and their wide use in the development of experimental platforms for microscale research. These techniques have been successfully applied to the production of reliable liquid cells that ensure successful encapsulation of thin solution specimens with minimal compromise in the resolution of TEM. Conventional TEM has rapidly advanced and is now one of the standard analytic tools in a wide range of research areas.[7] Implementation of TEM has been further augmented with the development of aberration correctors and direct electron-detecting techniques. The concurrent progress in liquid-cell fabrication and TEM apparatus has enabled the direct observation of chemical reactions in liquids with sub-nanometer resolution.

In principle, TEM observations are conducted by measuring the elastic and inelastic interactions of an electron beam that is transmitted through a specimen. The beam is housed in a vacuum environment with a pressure $<10^{-4}$ Pa to minimize unwanted electron–gas interactions. Therefore, perfect sealing of the liquid cells is a prerequisite for successful imaging in this ultrahigh-vacuum condition. In addition, the electron-beam-transparent windows and encapsulated liquid should be thin enough to minimize electron-beam scattering and ensure the high spatial resolution of the TEM observation. Liquid cells prepared by thin-film and microfabrication processes enable the isolation of liquid samples from the vacuum environment. With the development of high-performance detectors, magnetic lenses, and aberration correctors, liquid cells allow fast (millisecond scales, up to ≈400 frames per second) and high-resolution imaging of specimens in solution. The successful use of liquid cells in TEM observations has been demonstrated in many reports, confirming the potential as an in situ imaging method. Consequently, it is gaining much interest from researchers in various disciplines spanning from chemistry to materials science and even biology.[8–12]

Among the various research areas, nanoscience and nanotechnology is one of the most rapidly growing fields where TEM-based analysis is indispensable.[13–15] This is because

Dr. B. H. Kim, Dr. J. Yang,[+] D. Lee, B. K. Choi, Prof. T. Hyeon, Prof. J. Park
Center for Nanoparticle Research
Institute for Basic Science (IBS)
Seoul 08826, Republic of Korea
E-mail: jungwonpark@snu.ac.kr
Dr. B. H. Kim, Dr. J. Yang, D. Lee, B. K. Choi, Prof. T. Hyeon, Prof. J. Park
School of Chemical and Biological Engineering
Institute of Chemical Processes
Seoul National University
Seoul 08826, Republic of Korea

The ORCID identification number(s) for the author(s) of this article can be found under https://doi.org/10.1002/adma.201703316.

[+]Present address: Materials Sciences Division, Lawrence Berkeley National Laboratory, Berkeley, California 94720, USA

TEM provides information on the morphology, crystal structure, chemical composition, and elemental distributions at the sub-nanometer scale. Nonetheless, ex situ characterization methods, including conventional TEM analysis, still limit our understanding of colloidal nanoparticle growth and behavior, as most inorganic nanoparticles are synthesized and applied in the solution phase.[16,17] Moreover, their chemical and physical behavior change when they are isolated from the native solution for ex situ analysis. As a representative example, the formation mechanism of nanoparticles has been explained by the classical crystallization theory,[18] supported by conventional ex situ analysis including TEM, X-ray diffraction (XRD), and optical spectroscopy.[19,20] In the classical model, nuclei are formed at the early stage and grow to large particles by monomer attachment in the growth regime. However, there is significant evidence indicating that the situation is more complex than expected and that the formation of nanoparticles deviates from the classical nucleation and growth model.[21] For example, many kinds of prenucleation intermediate species (e.g., clusters) can be involved in nanocrystal synthesis.[22–31] Consequently, the development of novel characterization tools that can be used to observe nanoscale phenomena in solution with high spatial and temporal resolutions to obtain mechanistic answers to chemical reactions involving colloidal nanoparticles, is highly desirable. In this aspect, liquid-phase TEM is considered as cutting-edge in studies for growth, dynamics, and transformations of colloidal nanoparticles.

Here, we present the recent advances of using liquid-phase TEM for studying colloidal inorganic nanoparticles. The basics of liquid-cell design, a prerequisite for liquid-phase TEM measurements, are introduced. Then, research on the formation and transformation of nanoparticles is summarized. We also introduce TEM observations of nanoparticle motion in liquid cells. Finally, in situ TEM studies for electrochemical cells are briefly presented.

2. Technological Development

2.1. Liquid-Cell Design

Technically, the use of liquid cells as a method for encapsulating specimens in the conventional workflow of TEM enables imaging of events in the liquid phase by TEM. An appropriate design of liquid cells is one of the most important prerequisites for liquid-phase TEM. The representative structures of liquid cells are displayed in **Figure 1**. These include liquid cells manufactured from the microfabrication of silicon wafers and graphene liquid cells. Regardless of the different designs and materials used for fabricating liquid cells, the major components are tight-sealing for vacuum isolation, a space where the liquid-phase reaction takes place, and electron-beam-transparent windows for clear visualization. Depending on the experiment of interest, an additional compartment, such as electrodes, can be appended.

The typical design of static cells based on the microfabrication of silicon chips is displayed in Figure 1a.[32,33] Microfabricated liquid cells consist of top and bottom silicon chips whose lateral size is similar to that of normal TEM grids. The

Byung Hyo Kim received his B.S. (2006) and Ph.D. (2013) from the School of Chemical and Biological Engineering at Seoul National University. He is now a senior researcher of the Institute for Basic Science, working with Prof. Taeghwan Hyeon and Prof. Jungwon Park. He is currently working on the characterization of nanocrystals using liquid-phase TEM.

Jiwoong Yang received his B.S. (2011) and Ph.D. (2016) from the School of Chemical and Biological Engineering at Seoul National University. During the course of his Ph.D., he worked on the synthesis and applications of semiconductor nanocrystals under the supervision of Prof. Taeghwan Hyeon. He was a postdoctoral researcher at the Institute for Basic Science, working with Prof. Taeghwan Hyeon and Prof. Jungwon Park. He is now a postdoctoral researcher at the Lawrence Berkeley National Laboratory, studying in situ liquid-phase TEM.

Jungwon Park received his B.S. (2003) from the Department of Chemistry at Pohang University of Science and Technology, South Korea. He received his Ph.D. (2012) from the Department of Chemistry at University of California, Berkeley. After his Ph.D., he joined the research group led by Prof. David A. Weitz in the School of Engineering and Applied Sciences at Harvard University. In 2016, he started a faculty position as an Assistant Professor in the School of Chemical and Biological Engineering, Seoul National University. He is jointly affiliated to the Center for Nanoparticle Research, Institute for Basic Science. His research area includes in situ study of nanomaterials, liquid-phase TEM, phase transitions, interface chemistry, and low-dimensional materials.

windows are usually made with thin Si_3N_4 membranes with a thickness range of 10–100 nm to ensure high transmittance for the electron beam. The chips are separated by metal spacers, frequently made by deposition of indium or gold compounds. These provide a space to store the desired volume of the liquid
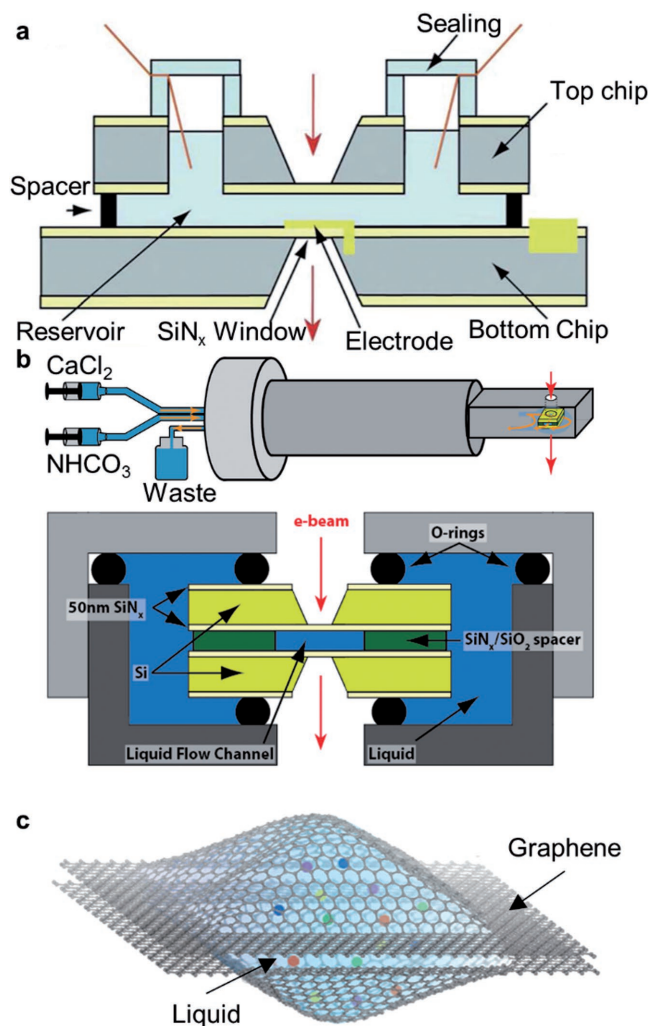
Figure 1. Representative structure of liquid cells. a) Typical design of a static-type microfabricated silicon cell. b) Schematic illustration describing a flow-type microfabricated silicon cell system. c) Schematic illustration of a graphene liquid cell. a) Reproduced with permission.[35] Copyright 2012, Royal Society of Chemistry. b) Reproduced with permission.[37] Copyright 2014, American Association for the Advancement of Science. c) Reproduced with permission.[38] Copyright 2012, American Association for the Advancement of Science.

sample. The microfabricated cells exhibit advantages including high reproducibility, high strength, and easy and precise modification of the cell design through well-developed fabrication techniques. Simple modification of these cells enables in situ study of electrochemical and/or temperature-controlled reactions in TEM.[8,34,35]

The microfabricated cells can be modified to flow-type liquid cells.[1,36,37] Many chemical reactions require the controlled introduction of chemical reagents when the retention time and temperature are settled. These are also needed for in situ TEM observation of reactions, which require sophisticated control of the reactants. For example, precipitation needs a continuous supply of the precursor solution. A typical structure of flow-type cells and a holder system is illustrated in Figure 1b. The basic structure is similar to static-type silicon cells, except for

implementation of flow inlets and outlets. The reactant liquid can be injected from the outside of the TEM and the flow can be controlled by a syringe pump system. O-ring sealing provides vacuum isolation in the reaction chamber during the measurement. In addition, these cells enable the simultaneous introduction of multiple reagents via multiple inlets. Flow-type cells significantly expand the range of chemical reactions that can be investigated by liquid-phase TEM.

Liquid cells can be also made by using thinner beam-transparent window materials, such as graphene.[38–40] The schematic illustration for a graphene liquid cell is displayed in Figure 1c. In this cell, liquid pockets are placed between two graphene sheets that are supported by TEM grids. Two graphene sheets adhere together by van der Waals' interactions such that the liquid pockets are preserved under a vacuum environment. Compared to microfabricated cells, graphene cells provide higher spatial resolution in liquid-phase TEM due to minimized electron-beam scattering by the window materials. Because graphene windows are much thinner (<1 nm) than those made from Si_3N_4 (10–100 nm), they are more transparent to the electron beam. In addition, the graphene liquid cells are less affected by the thermal and charging effects of the incoming electron beams. This is due to the high thermal and electrical conductivity of graphene.[33] Thus, graphene cells help high-resolution imaging of liquid-phase TEM observations.

Despite the well-established features and use of the above-mentioned liquid cells, there are still several features to be considered for reliable liquid-phase TEM observations. In principle, the resolution of liquid-phase TEM is determined by multiple factors, including the speed of motion and material changes in solution, the thickness and viscosity of the liquid media, the capture rate of the imaging camera, and ionization damage. A thick liquid scatters the electron beam, reducing the resolution of the acquired image. The presence of the imaging electron beam itself also requires careful consideration. This can potentially affect the chemical conditions of both the solvent and the nanoparticles and it can be manipulated to promote the desired chemical condition during in situ imaging. Thus, understanding of the beam effect is a prerequisite for liquid-phase TEM studies (see Section 8 for details). For example, the electron beam can decompose solvent molecules into radicals and cause either reduction or oxidation of reagents. A recent study demonstrating that graphene liquid cells help to control the oxidation reaction by hydroxyl radicals is encouraging.[33] The generation of radicals is effectively suppressed by the presence of graphene and its derivatives. This result highlights the importance of a cell design that can actively handle radiation chemistry by electron-beam irradiation. As described above, the imaging resolution with Si_3N_4 windows is low compared to that of graphene cells because of the high degree of electron scattering by the Si_3N_4 window. On the other hand, graphene cells also have limitation that it is difficult to generate defined shapes and distribution of liquid pockets. Therefore, future efforts are needed to develop advanced liquid-cell designs that ensure the encapsulation of a liquid sample in a chamber. These should exhibit precisely determined dimensions and minimize unwanted scattering and side reactions by the electron beam by using thin and conducting window materials.

ADVANCED
SCIENCE NEWS
www.advancedsciencenews.com

ADVANCED
MATERIALS
www.advmat.de

2.2. The Transmission Electron Microscope for In Situ Studies

For successful in situ TEM observation of liquid-phase phenomena, important breakthroughs have been made by technical development of TEM, including implementation of an aberration-corrector and a direct electron detector. The ability to capture high-resolution images within a short period of time is required to capture critical steps of continuous chemical reactions because the images are averaged during the acquisition time. As the acquisition time for a single frame of the image is extended, the acquired images will be blurred due to averaging of dynamic changes in the samples over the acquisition time. Generally, conventional TEM with charged coupled device cameras has the exposure time of a range from 0.1 to 1 s for a single image frame. This method inherently has a time delay during data transfer in multiple steps to produce a TEM image, which includes: (i) the conversion of the incident electron into photons, (ii) the projection of these photons onto the sensors, and (iii) the conversion of these photons into electric signals. The recently developed direct electron-detection technique can capture incoming electrons without loss of information such that it greatly enhances the signal-to-noise ratio and time resolution.[41] With the direct electron-detection method, a frame rate of 400 frames per second can be achieved with a 14 megapixel resolution and can be further accelerated by binning pixels.[12] In addition, the development of aberration-correcting lenses helps to acquire high-resolution images of specimens in liquid. In principle, aberration correctors allow a spatial resolution of 0.5 Å[42] and energy resolution of EELS of ≈1 eV.[43]

There is still a further demand for improving TEM techniques for the characterization of liquid samples. For example, one notable direction is development of ultrafast TEM. Although the time resolution of in situ TEM has been greatly improved, many of the critical steps of liquid-phase reactions occur at microsecond to nanosecond time scale. Recently, employing ultrafast TEM techniques has been demonstrated in studying rotational dynamics of colloidal nanoparticles. Through a short electron pulse with high current density, a time resolution of ≈10 ps was achieved with a spatial resolution of ≈10 nm.[44]

3. Nanoparticle Formation

There have been tremendous efforts for studies on in situ nanoparticle formation using liquid-phase TEM.[38,39,45–48] In particular, many of them focus on metal nanoparticles. These materials systems have several advantages over other types of materials such as semiconductors or metal oxides, including: (i) a mono-element composition that facilitates understanding of growth mechanism based on in situ TEM observations, (ii) a high Z-contrast that affords high-quality atomic resolution imaging in solution, and (iii) the ability to control nucleation, growth, and dissolution using an electron beam.

One of the pioneering studies in liquid-phase TEM was the formation process of copper metal nanoparticles in aqueous solution.[8] In this work, the nucleation and growth of copper nanoparticles were electrochemically induced on polycrystalline gold electrodes. The results revealed two distinctive periods corresponding to nucleation and growth, and each stage was well described by the classical crystallization model. Homogeneous nucleation occurred during the early stage of the reaction and was followed by diffusion-limited growth of the nanoparticles. In detail,[49] the growth period was divided into two stages, a 3D diffusion mode and a 1D planar diffusion mode, characterized by the change in the growth rate (R) from ≈$r^{0.5}$ to $r^{0.1}$ (**Figure 2**a).

With recent technical advances such as the employment of aberration correctors and direct electron detectors, the time and spatial resolution of in situ TEM measurements have been significantly improved. This improvement has led to the observation of important aspects of nanoparticle-formation processes (e.g., aggregative nucleation and growth) with atomic resolution. According to the classical crystallization theory, crystallization proceeds by the addition of molecular monomers into the crystal lattices, which is governed by the minimization of the Gibbs' free energy due to crystallization.[18] Sometimes, nucleation-and-growth processes include multiple intermediate steps rather than a direct transition from atoms to crystals. This scenario is categorized as nonclassical nucleation-and-growth behavior. The existence and role of prenucleation intermediates, including clusters and small nanoparticles, have been actively explored with in situ TEM in many studies. For example, Alivisatos and co-workers reported an in situ liquid-phase TEM study on the formation mechanisms of Pt nanoparticles and uncovered the coexistence of classical and nonclassical growth trajectories.[38,45] They suggested that the formation of Pt nanoparticles proceeded concurrently with the consumption of molecular monomers and the merging of the preformed smaller-sized Pt nanoparticles (Figure 2b,c). They also revealed that aggregation and shape reconstruction of Pt nanoparticles occur on time scales of hundreds of milliseconds and less than tens of seconds, respectively. In addition, they suggested that there is a critical concentration of nanoparticles above which aggregative growth becomes possible. These findings highlight the diversity in nanocrystal-formation pathways and reveal how aggregation of the prenucleation intermediate species contributes to the nanoparticle-formation process.

To gain a better understanding on how preformed nanoparticles grow into a single nanocrystal, particle formation by aggregation has been systematically studied by real-time observation.[38,45,50,51] The results suggest that there are two underlying mechanisms that thermodynamically govern the aggregative growth process by minimizing defects or misalignment between the preformed species. The first behavior was observed in the particle-to-particle interaction before particle aggregation.[38,45,50] When two nanoparticles are close together, they align to their crystallographic orientation by rotational or translational motion. On colliding along the aligned direction, they merge to form larger nanocrystals. An additional phenomenon to reduce the total energy of the merged nanoparticles was found after aggregation.[50,51] Once the nanoparticles merge together, spontaneous structural reconstruction occurs, which minimizes the free energy from the presence of defects or misalignment (Figure 2d). The concept of multistep nucleation and growth was also observed for Au nanoparticles in a
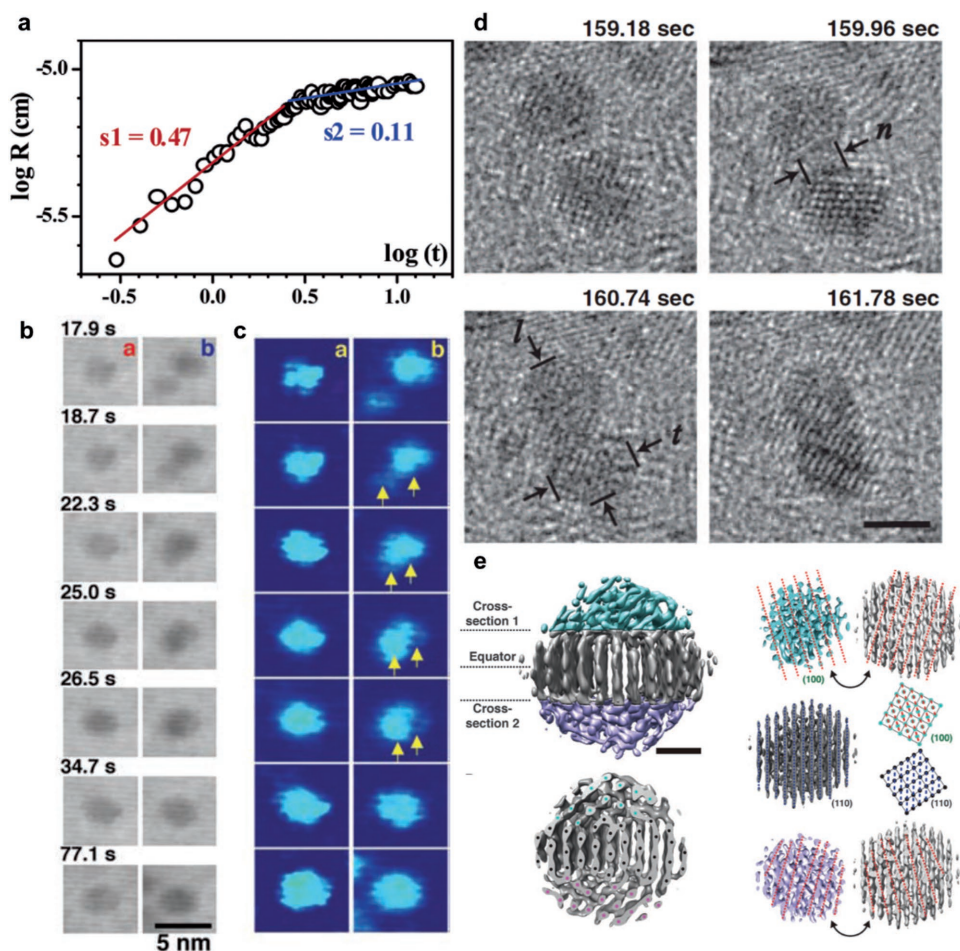
Figure 2. In situ observation of nanoparticle formation in liquid-phase TEM. a) Growth rate of copper nanoparticles on polycrystalline gold electrodes. b) In situ TEM images of a growing Pt nanoparticle displaying two representative pathways. The left and right columns illustrate growth by monomer addition and by coalescence, respectively. c) Enlarged color images (1.5×) of panel (b). d) In situ TEM images of the formation of a Pt nanoparticle by merging and reconstruction of two small-sized Pt nanoparticles (scale bar: 2 nm). e) 3D density map of a Pt nanoparticle and its slabs along several cross-sections. Data were acquired by reconstructing images of a rotating Pt nanoparticle in a liquid cell. The color coding represents the three domains in this nanoparticle (scale bar: 0.5 nm). a) Reproduced with permission.[49] Copyright 2006, American Chemical Society. b,c) Reproduced with permission.[45] Copyright 2009, American Association for the Advancement of Science. d) Reproduced with permission.[38] Copyright 2012, American Association for the Advancement of Science. e) Reproduced with permission.[59] Copyright 2015, American Association for the Advancement of Science.

recent study by Loh et al.[52] In this work, amorphous clusters are generated during the prenucleation stage, followed by crystallization. Additional evidence of nanocrystal formation through aggregative nucleation and growth was provided by investigating the atomic structure of the nanoparticles.[53–58] In particular, using liquid-phase TEM, near-atomic structures of individual Pt nanoparticles (<2 nm) were reconstructed (Figure 2e).[59] Because nanoparticles rotate freely in solution, it is possible to obtain high-resolution TEM snapshots in the versatile orientations of the particles with a direct electron detector. The afforded results suggest that a single Pt nanoparticle is composed of multiple domains that comprise twisted grain boundaries at their interface. These multiple domains make contact with the (100) and (110) surfaces at the grain boundaries to minimize the free energy associated with the plane defect at the interface.[60] These findings support the aggregative nucleation and growth model where the

crystallization process proceeds via merging of the smaller nanoparticle intermediates in the prenucleation stages. This is consistent with the previous understanding on the "oriented attachment" that has long been recognized in the field of geology.[61] Banfield and co-workers suggested that rather than being perfectly aligned along with their crystallographic orientations, various defects, such as twinning and dislocation, are favorably formed at the grain boundary of the merged crystals as a result of this attachment.[50,62–64]

Studies using in situ liquid-phase TEM have been successfully extended to the formation of more complex nanostructures such as core–shell.[65,66] The use of flow-type liquid cells is one of the effective ways to control heterogeneous growth. The formation of Au–Pd core–shell nanoparticles was investigated by introducing a mixture solution of preformed Au nanoparticles and PdCl$_2$.[67] Growth of Pd shells was induced by the reductive effect of the electron beam.

**ADVANCED
SCIENCE NEWS**
www.advancedsciencenews.com

**ADVANCED
MATERIALS**
www.advmat.de

4. Transformation of Nanoparticles

Chemical conversion of preformed nanoparticles to other forms of nanoparticles is an alternative way to produce nanoparticles with the desired composition and morphology that are difficult to synthesize directly from molecular-precursor solutions.[68–70] For example, Ag nanocubes were converted to Au nanocages by galvanic replacement reactions with Au ion.[71] CoS_2 hollow nanoparticles were synthesized from sulfidation of Co via the Kirkendall effect, induced by the difference in the diffusion rates of cations and anions in opposite directions.[72] Metal nanoparticles with high crystallinity were produced by selective etching, utilizing the high resistance of single-crystal nanoparticles to oxidative etching.[73,74] As most of these conversion processes have generally been investigated using ex situ analytical methods, the monitoring of their detailed mechanisms is nearly unexplored. Dynamic morphological changes during nanoparticle transformation can be visualized in real-time using the liquid-phase TEM technique.

4.1. The Kirkendall Effect

Hollow nanoparticles are of interest because of the high surface-to-volume ratio and large void space inside the particles. The hollow structure is formed from core–shell structures via the Kirkendall effect, which occurs between the core and shell with different ionic diffusion rates.[72,75–78] When the diffusion rate of the core atoms is faster than that of the shell atoms, void formation is initiated at the interface and subsequently grows into a large void that occupies the center of the particle. Several models, such as the steady-state bulk diffusion model and surface diffusion-mediated growth model, have been proposed to explain the Kirkendall effect. However, the mechanism of the hollowing process is not yet fully understood due to the lack of an in situ visualization method.[71,72,79] Using the recently developed liquid-phase TEM, the hollowing process can be monitored in real-time. Niu et al. observed the formation of Bi_2O_3 hollow nanoparticles using liquid-phase TEM under a controlled temperature.[80] Bi nanoparticles were generated from Bi precursors at 180 °C under an electron beam, followed by oxidation of the surface. Continuous oxidation led to the formation of hollow nanoparticles via the Kirkendall effect induced by fast outward diffusion of the Bi core atoms. The dynamics of Bi core diffusion were monitored in real-time by liquid-phase TEM. The diffusion coefficient for Bi nanoparticles is 7.56×10^{-18} m^2 s^{-1}, which is 3–4 orders of magnitude higher than that of the bulk. The high diffusion coefficient is explained by the defects in the intermediate state of the shells.

4.2. Galvanic Replacement

Galvanic replacement is a chemical reaction in which a metal with a low reduction potential is oxidized and dissolved, while other metal ions with high reduction potentials are reduced and deposited, in the presence of an electrolyte.[81,82] In 2002, Sun and Xia first reported a nanoscale galvanic replacement reaction between Ag nanocubes and Au ions.[71] Thereafter, a number of papers have reported that controlled dissolution and deposition via galvanic replacement can be used to produce various hollow nanoparticles with complex structures.[83–88] In addition to metal nanoparticles, galvanic replacement has also been reported in metal oxide nanoparticles.[79]

A galvanic-replacement reaction proceeds through the following mechanisms: (i) formation of pinholes on the surface of the template nanoparticles by etching, (ii) dissolution of the nanoparticles and formation of an alloy on the surface of the nanoparticle, and (iii) a dealloying process.[71] Conventionally, the galvanic-replacement mechanism was characterized by TEM images of sample aliquots. However, since quenching in galvanic replacement does not cease the reaction completely at the time of interest, in situ observation with liquid-phase TEM can be an indispensable alternative to provide a detailed reaction mechanism.

Sutter et al. first used a liquid-phase TEM to investigate the galvanic replacement reactions between Ag nanoparticles and an aqueous Pd salt solution.[89] In situ observation revealed that the Ag nanoparticles were transformed into a hollow Ag–Pd nanostructure in the presence of $PdCl_2$ (**Figure 3**a–c). The reaction rate of the galvanic replacement in the liquid-phase TEM study was faster than that monitored by an ex situ method. The difference is attributed by the electron-beam effect, i.e., reducing $(PdCl_4)^{2-}$ to Pd^0 by the electron beam, which accelerates the replacement reaction. Tan et al. also reported real-time imaging of galvanic-replacement reactions between silver nanocubes and $HAuCl_4$.[43] Since the galvanic reaction is usually completed within a few minutes, galvanic replacement would occur between sample preparation and measurement, before it can be captured by liquid-phase TEM imaging. In order to overcome this problem, a disodium salt of ethylenediaminetetraacetic acid (EDTA), a chelating agent, was used to slow the reaction. Liquid-phase TEM demonstrated that the surface of the Ag nanoparticles is etched first and Au is subsequently deposited.

4.3. Etching

The surface area of the nanoparticles is so large that they are easily etched in acidic and reactive environments.[90–92] Etching sometimes poses a problem when nanoparticles are used as catalysts. For example, in a fuel cell that operates well in an acidic environment, most alloy catalysts are easily etched, and their activity is significantly changed.[90] Etching is also an issue in bioengineering application of nanoparticles because they are easily etched away in the endosomes of cells with low pH. On the other hand, the etching process can be used to obtain the desired nanoparticle morphology.[73,74] In this regard, analyzing the etching process in real time is important for catalytic and biological applications of nanoparticles.[93,94]

Ye et al. tracked the process of etching Pt nanorods with $FeCl_3$ in a graphene liquid cell.[95] By the electron beam, $FeCl_3$ decomposed water molecules to generate radicals that facilitated etching of the nanorods. When the $FeCl_3$ concentration was low, etching proceeded in an equilibrium state and the most stable crystal facet was maintained during etching (Figure 3d,e). Conversely, when the $FeCl_3$ concentration was high, the system was in a nonequilibrium state and the Pt
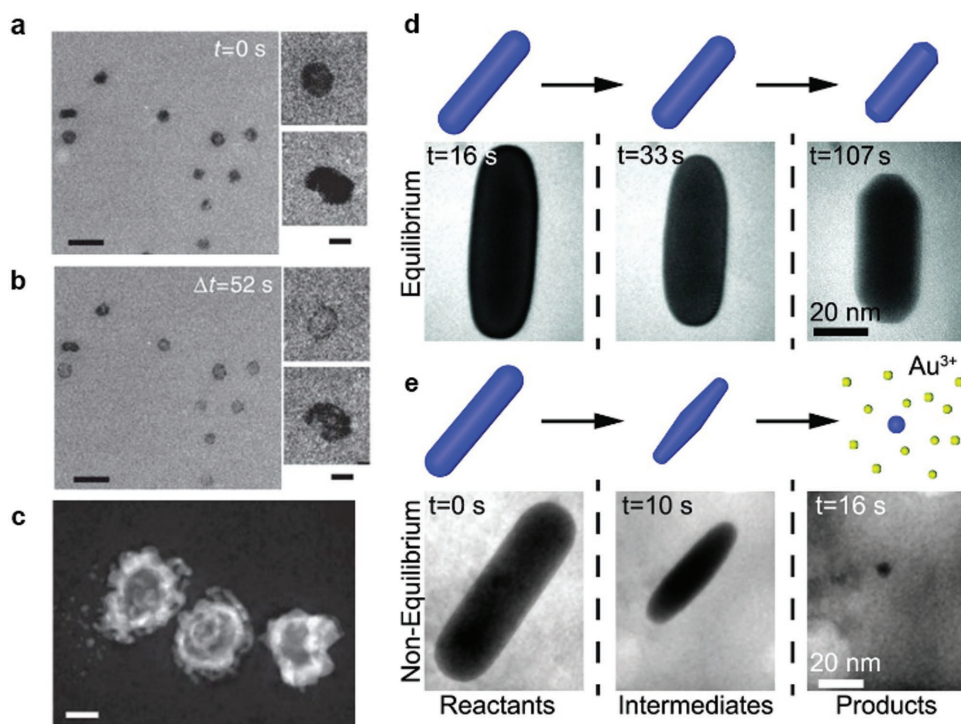
Figure 3. a–c) In situ TEM images tracking the galvanic replacement of Ag nanoparticles in an aqueous PdCl$_2$ solution. a) Initial TEM image of the Ag nanoparticles (scale bar, 100 nm) and magnified images of selected particles (right of panel, scale bar: 20 nm). b) The same batch of nanoparticles (scale bar: 100 nm) after the reaction and magnified images of selected particles (right of panel, scale bar: 20 nm). c) High-resolution Z-contrast image of the nanoparticles corresponding to panel (b). d) In situ TEM images of Au nanorods etched in the presence of concentrated FeCl$_3$. The rods were in near-equilibrium with flat {100} facets at their tips. e) In situ TEM images of Au nanorods etched in the presence of diluted FeCl$_3$. The images display the transition from nanorods to a nonequilibrium intermediate with sharp tips. a–c) Reproduced with permission.[89] Copyright 2014, Nature Publishing Group. d,e) Reproduced with permission.[95] Copyright 2016, American Association for the Advancement of Science.

surface was exposed to a large number of {211} crystal facets. Calculation by molecular dynamics supported these results.

5. Nanoparticle Motion

5.1. Motion of Single Nanoparticles

Nanoparticles exhibit continuous translational and rotational motion in liquid media. Although nanoparticle movement has been simulated with molecular-dynamics calculations,[96] real-time tracking of particle movement is a great challenge due to the absence of in situ visualization tools that can capture motions at the nanoscale level. Since liquid-phase TEM is a powerful technique for tracking trajectories of individual nanoparticles, diffusion dynamics of single particles and inter-particle interactions have been intensively studied using this analytical technique.[97–99]

The translational motion of a particle is traditionally described by Brownian motion and follows the Einstein–Stokes' equation (Equation (1))[100]

$$D = \frac{k_B T}{4\pi\eta a} \tag{1}$$

where D is the diffusion coefficient of a particle, k_B is the Boltzmann's constant, T is the temperature, η is the viscosity,

and a is the radius of the particles. For example, the diffusion coefficient of a spherical nanoparticle with a radius of 2 nm, in water, is 1×10^{-10} m^2 s^{-1}. From Equation (1), the diffusion coefficient of a particle depends on its size and the viscosity of the solvent. Several groups have used liquid-phase TEM to track the motion of nanoparticles by controlling their parameters and the solvent. Zheng et al. reported that diffusivity is negatively correlated to the size of the nanoparticles.[97] The effect of solvent viscosity on nanoparticle diffusion was also studied.[101] Gold nanoparticles, 30 nm in size, in a 20% water/80% glycerol mixture exhibited a diffusion coefficient of 7×10^{-18} m^2 s^{-1}. In contrast, the diffusivity of the same particles in 100 % water is 1.4×10^{-17} m^2 s^{-1}. Although the trend is in good agreement with the Einstein equation, the actual diffusivity of nanoparticles in a liquid-phase TEM is much slower than the theoretical value.[101,102] For example, a diffusion coefficient of Au nanoparticles coated with thiolated chitosan in a Si$_3$N$_4$ liquid cell is approximately fourfold slower than that of the theoretical estimation.

The slow movement of nanoparticles is attributed to the confined geometry of the liquid cells.[102] From a microscopic point of view, liquid molecules near the interface flow more slowly than those located away from the wall due to shear stress. In addition, the presence of interactions between the liquid molecules and the Si$_3$N$_4$ wall slows down the movement of the molecules near the wall.[101] In aqueous solution, the hydrogen atoms in the first layer of water may form hydrogen bonds with

the Si_3N_4 wall surface. As the water molecules interact with each other by hydrogen bonding, the bound water molecules in the first layer may influence the motion of several layers of water molecules, thereby increasing the viscosity. Some studies have suggested that the slow motion is induced by the phase separation of mixed solvents. When the solvent viscosity is significantly different and the nanoparticles are more soluble in a phase-separated solvent of higher viscosity, the movement of the nanoparticles becomes dull.[101]

During TEM measurements, the electron beam induces a positive charge onto the Si_3N_4 window and the induced surface charge affects the motion of the charged nanoparticles.[103,104] Liu et al. demonstrated that the movement of positively charged (cetyltrimethylammonium (CTA)) and negatively charged (citrate) gold nanoparticles is significantly different because of the positively charged window surface.[105] While negatively charged particles are fixed to the wall, even at a high electron-beam intensity, due to strong interactions with the positively charged wall, positively charged gold nanoparticles exhibit a smooth motion.

The irradiated electron beam causes stick-and-slip motion of nanoparticles, as well as retardation of nanoparticle movement. Since Si_3N_4 is a dielectric insulator, the charges induced by the electron beam are localized in the radiated spots of the Si_3N_4 wall. Thus, nanoparticles with induced dipoles are adsorbed onto the wall surface. Chee et al. discovered that gold nanoparticles exhibit sticky motion, so that the particles only move a few nanometers with rotational motion on the Si_3N_4 surfaces (**Figure 4**a,b).[103] When the absorbed nanoparticles were desorbed from the window with thermal vibration, they flew ≈50 nm and stuck again with fast pivoted rotations. In contrast to the stick-and-slip motion in the Si_3N_4 liquid cell, no such nanoparticle motion was observed in a graphene liquid cell.[104] Because of the high electron mobility of graphene, the induced charges easily dissipate into a lateral dimension. Thus, the lack of localized charges in graphene allows continuous motion of the nanocrystals.

Charged nanoparticles can be driven by the electric force of a strong electron beam. White et al.[106] observed that Pt nanoparticles in aqueous solution move outward from the center of the field of view. The higher the beam dose rate is, the faster the motion that is observed. This result indicates that the charging of an electron beam can control nanoparticle movement. The inductive effect of the electron beam has been applied to the nanoscale manipulation technique in so called "molecular tweezers".[107,108] When a high-energy electron beam (100–200 keV) is focused on a several nanometer-sized spots, the beam can trap and move nanoparticles (Figure 4c). van de Put et al. wrote letters with silica nanoparticles using the molecular-tweezers method (Figure 4d).[109] A review written by Zheng's group provides more detailed information regarding molecular tweezers.[107]

Another aspect of nanoparticle movement is rotational motion. Fu et al. observed rotational motion of Au dimer nanoparticles in a 300-nm-thick liquid cell.[110] When a pulse laser was incident on the liquid cell, the dimers began to rotate, and the motion was traced in nanosecond scale with an electron microscope. In contrast to the dimer, it is difficult to observe the rotational motion of spherical nanoparticles in isotropic

form using liquid TEM. In order to track the rotational motion of a spherical particle properly, the lattice planes of the particle should be clearly visible.[111] The use of graphene liquid cells enables high-resolution images of nanocrystals during their rotation that are attributed to the ultrathin nature of the graphene window.[38] A paper on 3D reconstruction using high-resolution TEM images of rotating nanoparticles was published in 2015.[59] In this work, Park et al. collected a number of high-resolution TEM images of individual Pt nanoparticles that rotate randomly in a graphene liquid cell. The ab initio 3D reconstruction algorithm that was developed for biomolecules was applied to the TEM image set of the nanoparticles to produce 3D structures of the individual nanoparticles. This technique shows great potential as a new tool to provide accurate structural information at an individual nanoparticle level.

5.2. Interparticle Interactions

In addition to Brownian motion, nanoparticle motion is affected by interparticle interactions. The presence of attraction forces between nanoparticles, originating from their dipole moment or van der Waals' forces, induces the particles to move closer together. The relative motion between nanoparticles perturbed by the interparticle interaction is one of the key factors to elucidate self-assembly and oriented attachment mechanisms (see Sections 5.3 and 6, respectively), consequently, real-time observation is critical for elucidation of the detailed dynamics.

Chen et al. statistically analyzed the relative trajectory of positively charged gold nanorods.[112] When the nanorods are close to each other, weak anisotropic interparticle interactions cause the nanorods to approach the tips of the adjacent nanoparticles selectively (Figure 4e–g). They also observed the relative trajectories of two nanoparticles connected by a linker.[113] By conjugating the Au nanoparticles with DNA, their relative temporal positions could be tracked by liquid-phase TEM.

Nanoparticle motion can also be influenced by interactions with other materials located in the vicinity. For example, the interaction of nanoparticles with biomaterials is an important issue in nanobiotechnology.[114,115] Pohlmann et al. conducted a proof-of-concept study on nanoparticle–cell interactions using liquid-phase TEM.[116] Figure 4h displays real-time observation of Au nanoparticles entering brain-tumor stem cells. Liquid-phase TEM shows great potential for applications in a wide span of research areas that require a mechanistic understanding of biological processes based on high-resolution microscopy observations.

5.3. Self-Assembly

Self-assembly has been extensively utilized for applications of nanoparticles in electronic devices, magnetic storage media, photonic crystals, and biological sensors.[15,117–121] Self-assembly is caused by different factors including attractive interactions between nanoparticles originating from van der Waals' forces, as well as dipole moments in nanoparticles, depletion forces, and solubility change of the nanoparticles during solvent drying or salt addition. To date, small-angle X-ray scattering
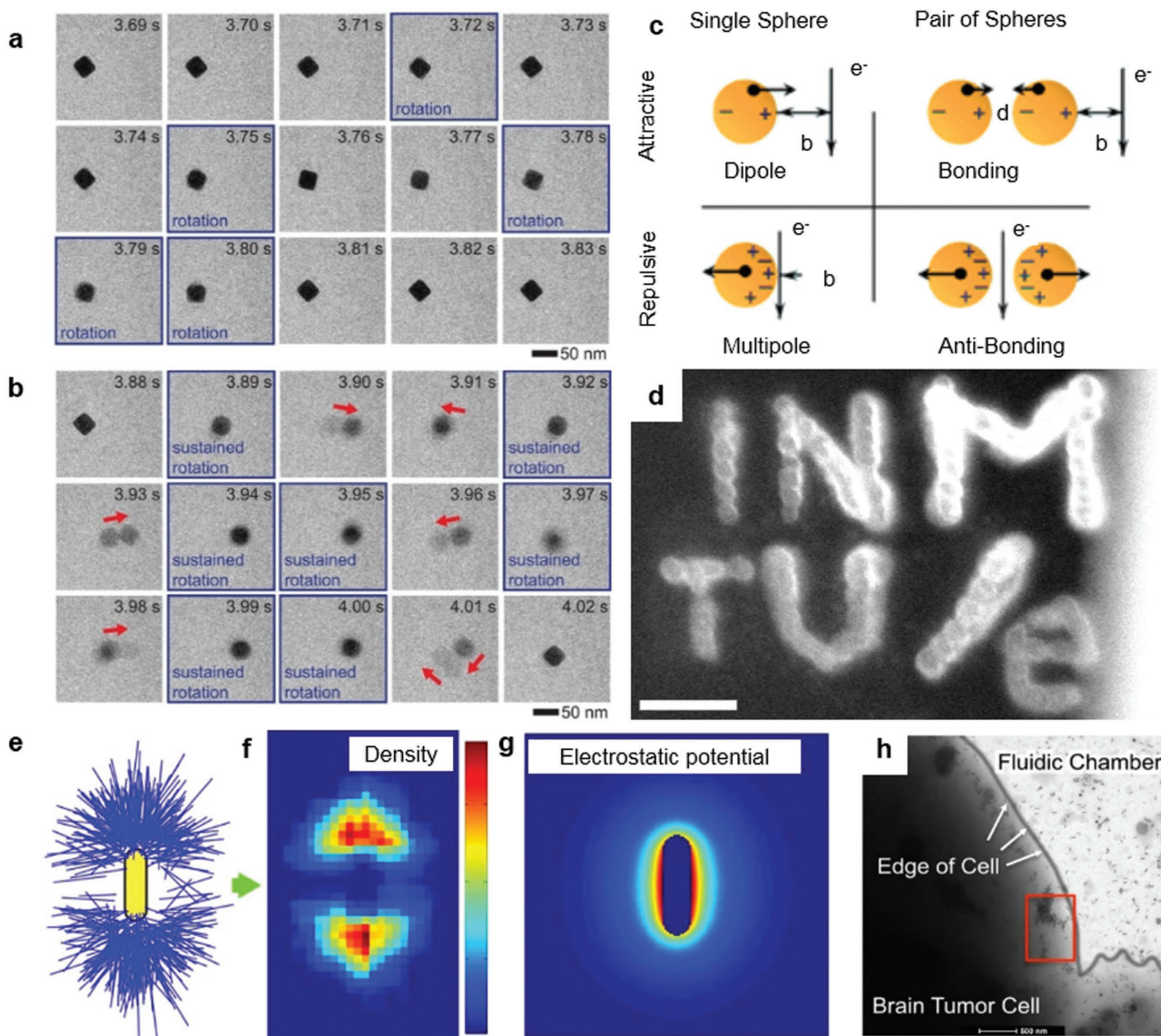
**ADVANCED
SCIENCE NEWS**
www.advancedsciencenews.com

**ADVANCED
MATERIALS**
www.advmat.de

Figure 4. a) Time-series TEM images of nanoparticles in the "stick" mode where the nanoparticles move in small displacements. b) TEM images of nanoparticles in the "flight" mode where the nanoparticles move long displacements (≈50 nm) within a single frame (highlighted with red arrows). c) Particle motion in the presence of a focused electron beam. d) Dark-field STEM image of silica particles written by the "molecular tweezers" method (scale bar: 500 nm). e–g) Comparison of experimental data and theoretical modeling of electrostatic interactions. e) Position plot of attached nanorods on an individual nanorod. f) The observed density of rods corresponding to panel (e). g) Energy contour map calculated for a pair of nanorods, where one particle is fixed vertically at the center. The potential is color-coded: red for high potential and blue for low potential. h) A TEM image of a brain tumor cell incubated with gold nanorods. The image indicates great internalization of nanorods in select regions. a,b) Reproduced with permission.[103] Copyright 2016, American Chemical Society. c) Reproduced with permission.[107] Copyright 2013, Royal Society of Chemistry. d) Reproduced with permission.[109] Copyright 2015, Wiley-VCH. e–g) Reproduced with permission.[112] Copyright 2015, American Chemical Society. h) Reproduced with permission.[116] Copyright 2015, American Chemical Society.

(SAXS) has been mainly used for real-time analysis to investigate self-assembly mechanisms.[122–124] However, interpretation of SAXS data that converts structural information from a reciprocal lattice space to real space is complicated and somewhat unreliable, such that phase information is frequently lost during the data-conversion process. Therefore, real-time information directly obtained from liquid-phase TEM can enhance our understanding of nanoparticle self-assembly.

Park et al. reported the direct observation of a self-assembly process of Pt nanoparticles by solvent-drying using a Si_3N_4

liquid-phase TEM.[125] During solvent evaporation, the nanoparticles are dragged along the solvent front and gather into amorphous agglomerates (**Figure 5**a). These agglomerates are subsequently crystallized by local fluctuation. As the assembly proceeds, the coordination number increases, while the area incorporating the nanoparticles decreases. The following paper reported that the roles of solvent drying differ with different initial nanoparticle concentrations.[104] For example, at high initial nanoparticle concentrations, they are spread two-dimensionally as the liquid thickness becomes thinner; this results in
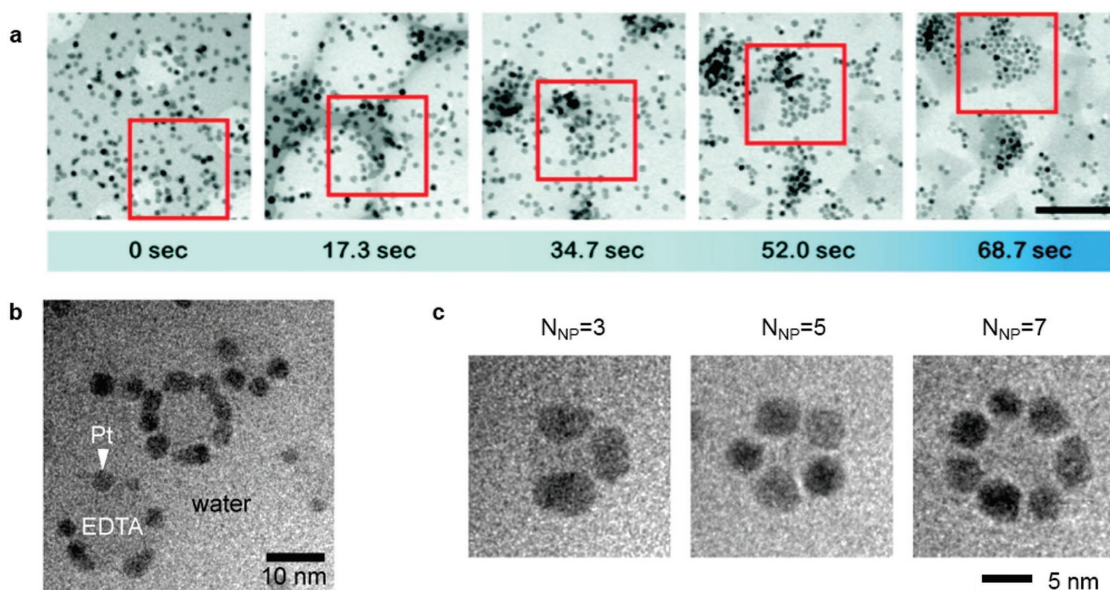
Figure 5. a) Time-series TEM images of superlattice formation during solvent drying (scale bar: 100 nm). b) Nanoparticle assembly in the periphery of a nanodroplet composed of EDTA in aqueous solution. c) TEM images of the nanoparticle assembly on the interface between water and EDTA nanodroplets of three different sizes. a) Reproduced with permission.[125] Copyright 2012, American Chemical Society. b,c) Reproduced with permission.[129] Copyright 2016, American Chemical Society.

a decrease in the local density of the particles. The motion of other types of nanoparticles such as PbSe were also studied in the same report.

The dipole moment in nanoparticles is one of the key components that determines self-assembly dynamics. Dispersed FePt nanoparticles are reported to initially form 1D chain structures and subsequently evolve into 2D self-assembled structures.[126] Since FePt is a superparamagnetic material with magnetic dipoles, a chain arrangement forms as the intermediate state. The long-range force between the nanoparticles was quantitatively analyzed.

Charged nanoparticles are well dispersed in hydrophilic solvents due to their repulsive interactions. However, once the particles lose their charges, they become unstable and tend to assemble by themselves. Liu et al. discovered that nanoparticles charged with CTA^+ ions aggregate during in situ TEM measurements in solution.[105] The electrons are projected to positively charged gold nanoparticles and fill the trapping sites. This generates an anisotropic polaronic state, leading to chain formation. In addition, the electrons reduce CTA^+ to low charge density, causing the nanoparticles to become unstable. Small nanoparticles are assembled faster than the large nanoparticles, since they are more susceptible to reduction by the electron beam because of fewer CTA^+ ions on their surface. It was also observed that hematite nanoparticles are agglomerated by salt in the aqueous solution.[127] Aggregation promoted by an increase in ionic strength provides direct confirmation of the Derjaguin–Landau–Verwey–Overbeek (DLVO) theory.

It is known that nanoparticles are well assembled at the interface of two different solvents or phases by surface tension.[128] Lin et al. illustrated the process of assembling Pt nanoparticles at a water/nanodroplet (EDTA) interface using liquid-phase TEM.[129] As an external nanoparticle approaches to a droplet on which nanoparticles are assembled, the preassembled particles move slightly along the circumference to provide space for the incoming nanoparticle. The external nanoparticle enters this empty space and becomes assembled. Through this process, the number of nanoparticles per droplet reaches a constant, depending on the size of the nanodroplets (Figure 5b,c).

Sutter et al. reported the self-assembly process of octapod-shaped nanoparticles in liquid-phase TEM.[130] Kim et al. investigated the behavior of a premade self-assembled structure in the presence of an electron beam,[131] whereby gold nanoprisms (89 nm × 7.5 nm) spontaneously self-assemble due to their unique shape. When an electron beam was applied to the nanoprisms, they were charged and the interparticle distance widened. The change was observed with in situ TEM and supported by SAXS spectra.

6. Attachment Between Nanoparticles

As discussed in Section 5.2, attractive interactions between nanoparticles move them closer together. When the ligand density of the nanoparticles is low and their surface energy is high, they attach directly to the adjacent nanoparticles. As discussed in Section 3, attachment also occurs during the nanoparticle growth process where small nanoparticles aggregate and fuse to grow into larger nanoparticles.[50,132]

If crystal planes of two nanocrystals are perfectly matched during the attachment, they are subject to undergoing "oriented attachment."[133] When this occurs continuously along a 1D direction, anisotropic nanomaterials can be obtained.[134–136] For PbSe nanocrystals, oriented attachment results in PbSe thin films without grain boundaries.[122,137–142] The assembled nanocrystalline films exhibit high electron mobility due to their
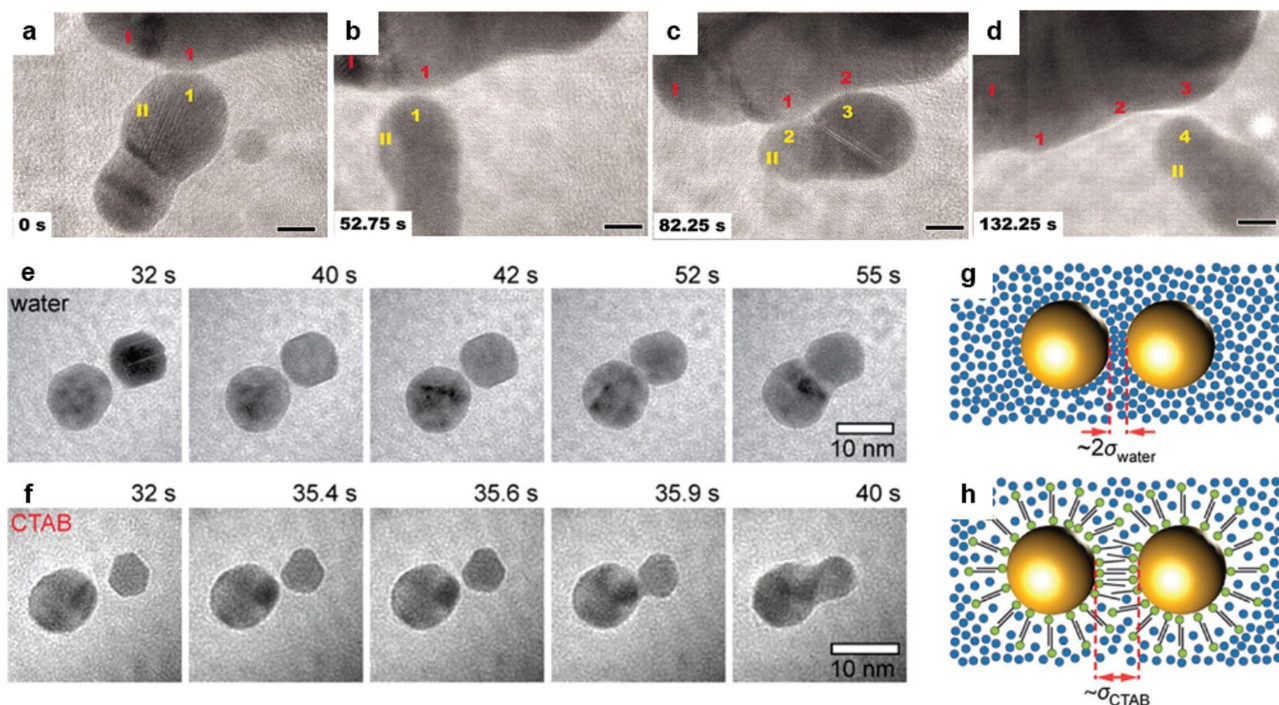
**ADVANCED
SCIENCE NEWS**

www.advancedsciencenews.com

**ADVANCED
MATERIALS**

www.advmat.de

Figure 6. a–d) Time-series TEM images of two iron oxyhydride nanoparticles (particle I and II) illustrating the typical dynamics of lattice finding and matching (scale bars: 10 nm). e,f) Time-series TEM images of pairwise interactions of gold nanoparticles without ligands (e) and with CTAB ligands (f). g,h) Schematic diagram of the position of the molecules corresponding to panels (e) and (f), respectively (blue spheres, water molecules; orange spheres, gold nanoparticles; yellow, CTAB). a–d) Reproduced with permission.[50] Copyright 2012, American Association for the Advancement of Science. e–h) Reproduced with permission.[145] Copyright 2016, American Chemical Society.

crystallographic coherence at the atomic level.[143,144] However, how a nanocrystal finds and matches the crystal planes of an adjacent nanocrystal was unknown until liquid-phase TEM was developed.

Liquid-phase TEM provided an interesting answer for this.[50] **Figure 6**a–d illustrates that an iron oxyhydride nanocrystal approaches another nanocrystal and stops at a fixed distance. The nanoparticle continues to rotate until it finds the preferred lattice direction. Subsequently, a point contact is formed abruptly between the two nanoparticles, followed by atom-by-atom oriented attachment at the contact point. Moreover, the Au nanoparticles are also found to hold a certain distance from each other before they are attached.[145] This behavior was consistently observed in nanoparticles with and without cetyl-trimethylammonium bromide (CTAB) ligands. Interestingly, the proximity distance between the CTAB-capped nanoparticles is similar to the length of the intercalated ligands (Figure 6e–h). For bare nanoparticles, the distance is approximately twice the size of the water molecule. This leads to the hypothesis that a hydrate double layer is formed between the two nanoparticles when they are close to each other. Subsequently, such geometry was confirmed to be energetically stable by molecular dynamics. Thereafter, a sudden jump to contact and orientated attachment occurs, similar to that observed by Li et al. (Figure 6a–d).[50]

Aabdin et al. proposed another scenario by examining the attachment of Au nanocrystals using liquid-phase TEM. They suggested that the angle at which the two nanocrystals meet is critical for achieving oriented attachment.[146] When the two gold nanocrystals meet at a small angle (<15°), the nanocrystals

are able to rotate to some degrees and match the crystal plane (**Figure 7**). When the two nanocrystals meet at a large angle (>15°), dislocation occurs. The importance of the contact angle between the nanocrystals was validated by molecular-dynamics simulation.

On the other hand, linker-mediated attachment of nanoparticles was observed with liquid-phase TEM.[147] Linear and branched networks are formed from gold nanoparticles coated with ethylene diammonium. The spacing between the nanoparticles was determined as 1.5 nm, consistent with the sum of the lengths of the two surfactants and the length of one linker molecule.

7. In Situ Study of Nanomaterials with External Bias

Nanomaterials are used as an important component in electrochemical devices composed of cathodes,[148–153] anodes,[154–159] and electrolytes.[160–165] The working mechanisms of electrochemical cells have been studied by ex situ methods.[166–176] However, these studies cannot answer questions related to electrolyte decomposition and formation of the solid electrolyte interphase (SEI). In order to answer such questions by in situ observation, an open-cell configuration for TEM has been developed (**Figure 8**a).[177–180] As a model experiment, $LiCoO_2$ (cathode) and SnO_2 (anode) nanowires were connected to a droplet of ionic liquid and an external potential was applied to this open-cell through a biasing system.[177] Because
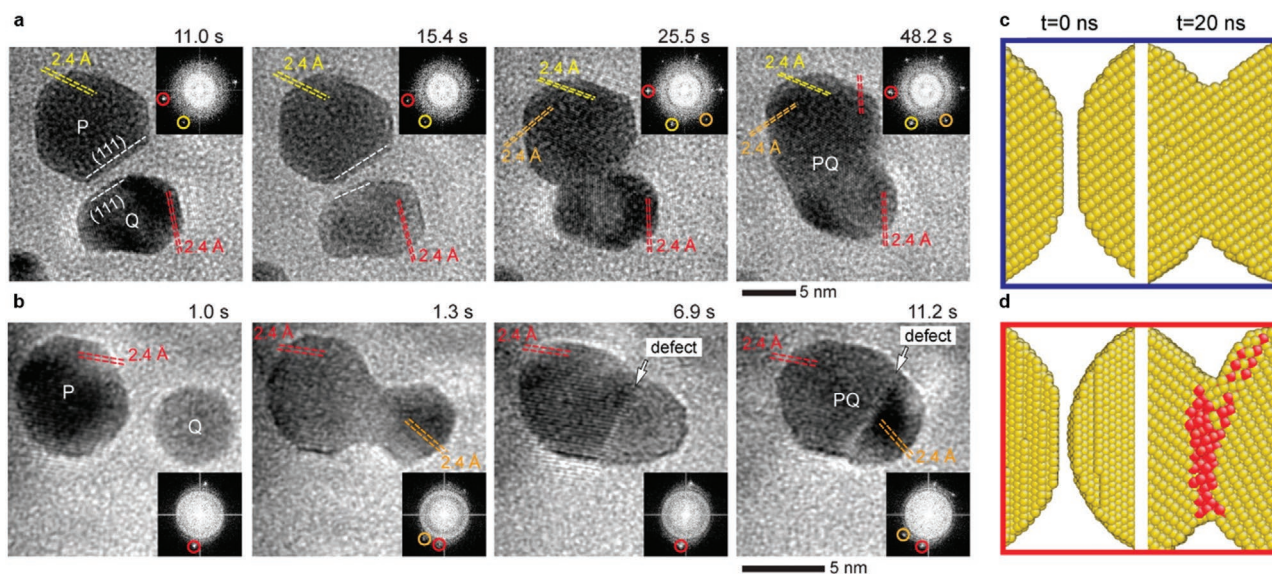
**ADVANCED
SCIENCE NEWS**
www.advancedsciencenews.com

**ADVANCED
MATERIALS**
www.advmat.de

Figure 7. a,b) Time-series TEM images of coherent bonding between two gold nanoparticles that make contact with a small angle of ≈9° misalignment (a) and defect-mediated bonding between two gold nanocrystals that make contact with a large angle (b). c,d) Molecular dynamics simulations of coherent bonding (c) and defect-mediated bonding (d). The red atoms indicate defects. Reproduced with permission.[146] Copyright 2014, American Chemical Society.

conventional electrolytes evaporate in the high vacuum in TEM, a nonvolatile ionic liquid or solid electrolytes were used in this study. However, the use of ionic-liquid electrolytes requires a higher overpotential than the actual battery system, resulting in a change in kinetics. To avoid problems posed by an open-cell configuration, a closed-cell (liquid cell) configuration was developed (Figure 8b).[181–183] In this configuration, a full cell composed of two electrodes and a liquid electrolyte is sandwiched between two electron-transparent windows and sealed to prevent evaporation of the electrolyte in high-vacuum TEM. Several in situ TEM studies of electrochemical cells using conventional liquid electrolytes have been reported.[184–188] Gu et al. observed lithiation and delithiation of silicon-nanowire electrodes in the same environment as a commercial battery system where a conventional liquid electrolyte and Li metal were applied.[183] Real-time analysis of the SEI layer is also important to improve battery stability and efficiency because the SEI layer plays a critical role in stabilizing electrodes and creating a path for Li ions between the electrodes and the electrolyte.[189–193] Sacci et al. studied the formation and decomposition mechanisms of the

SEI layer during charging and discharging by using a closed-cell system with a conventional Au electrode and $LiPF_6$ ethyl carbonate/dimethyl carbonate electrolyte.[189] The closed cell still has limitations of relatively low resolution and electron-beam effect that should be overcome in the future.

8. Influence and Manipulation of the Electron Beam in Liquid-Phase TEM

To gain a better understanding of observations by the liquid-phase TEM, it is important to understand the effects of the electron beam on liquid samples. Furthermore, quantitative controls over chemical and physical interactions between inherent electron beam and solvent molecules can allow desired chemical conditions to be generated during in situ TEM imaging. Regardless of the types of solvents used in the TEM experiments, most liquids are subject to decomposition by the electron-beam bombardment; as a result, radical species, a pH change of the solution, and charging of the species in the
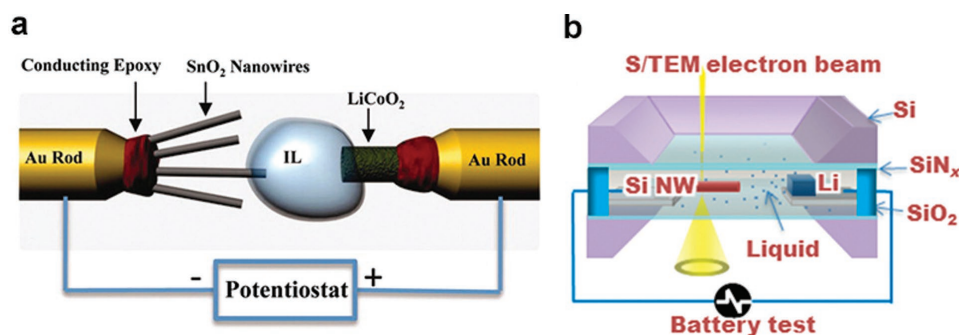

Figure 8. a,b) Schematic diagrams of an open cell (a) and a closed liquid-cell battery (b) for liquid-phase TEM. a) Reproduced with permission.[174] Copyright 2010, American Association for the Advancement of Science. b) Reproduced with permission.[183] Copyright 2013, American Chemical Society.

solution are generated. Most of these electron-beam effects are mainly due to the radiolysis of the solvent molecules by inelastic electron scattering.

The effects of the radiation on water are well documented in classical radiation chemistry.[194] Although the dose rate of the electron beam employed in the TEM measurement is significantly high, compared to that of the process in conventional radiation chemistry, information from radiation chemistry provides fundamental elements to understand radiolysis in liquid-phase TEM experiments. Water molecules (H_2O) can be decomposed into various kinds of radicals including aqueous electrons (e_{aq}^-), hydroxyl radicals ($^\bullet OH$), and hydrogen radicals ($^\bullet H$) by the beam irradiation and these radicals further stimulate formation of byproducts such as H_2, H_3, OH^-, H_2O_2, HO_2^-, and H_3O^+ (**Figure 9**a). Aqueous electrons (e_{aq}^-), hydroxyl radicals ($^\bullet OH$), and hydrogen radicals ($^\bullet H$) are of particular interest, because they have a strong reducing (e_{aq}^-, $^\bullet H$) or oxidizing ($^\bullet OH$) strength. Basically, most of the nucleation and growth events of the metal nanoparticles that take place in the liquid TEM measurement are governed by the redox reaction (Figure 9b).

Interactions between the electron beam and organic solvents are also important because a variety of colloidal nanomaterials have been synthesized in organic solvents. The beam effect is much more complicated to understand in organic solvents because a larger number of different chemical species can be generated than those produced in water under electron-beam irradiation. The products of radiolysis include a wide range of chemicals, such as gas molecules, small organic species, dimeric species, and polymeric species. Radicals are also produced by beam irradiation in organic solvents. As in water, strong reducing radicals, e_{aq}^-, and strong oxidizing radicals, which have analogous roles to $^\bullet OH$ in water, are generated in organic solvents.

Interestingly, several recent studies have demonstrated that the redox reaction induced by the electron beam can be controlled in a variety of ways. One simple approach is to adjust the dose rate of the electron beam, which controls the
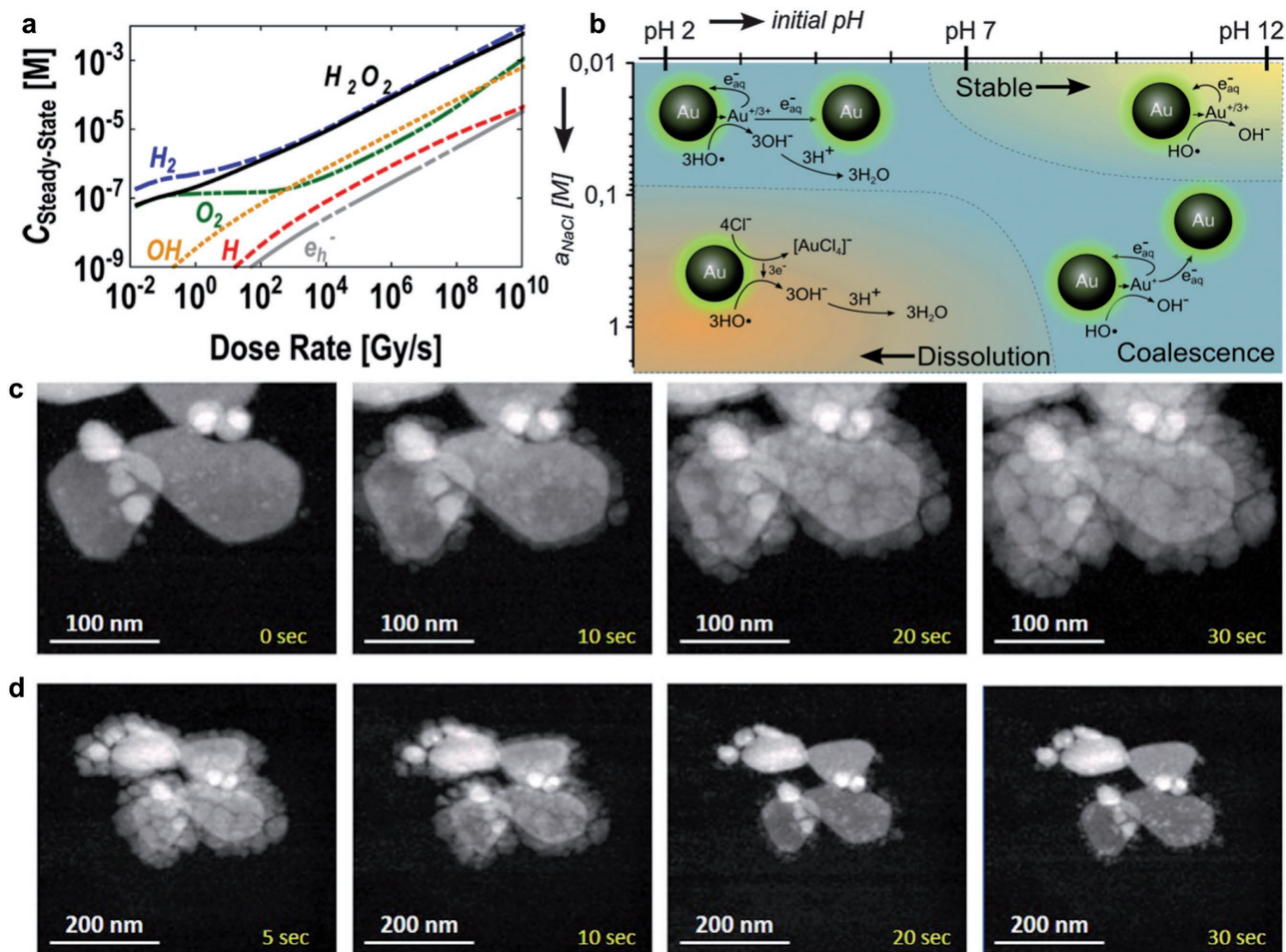

Figure 9. a) Steady-state concentrations of various chemical species produced by radiolysis (deaerated, neat water). b) Proposed reaction mechanism of Au nanoparticles in water under beam irradiation according to the Cl^- concentration and pH. c,d) Time-series STEM images of growth (reduction reaction; dose rate = 6.1 e^- $Å^{-2}$ s^{-1}) (c) and dissolution process (oxidation reaction; dose rate = 1.5 e^- $Å^{-2}$ s^{-1}) (d) of Cu shells on Au nanoparticles. a) Reproduced with permission.[195] Copyright 2014, American Chemical Society. b) Reproduced with permission.[197] Copyright 2015, Royal Society of Chemistry. c,d) Reproduced with permission.[196] Copyright 2017, Royal Microscopical Society.
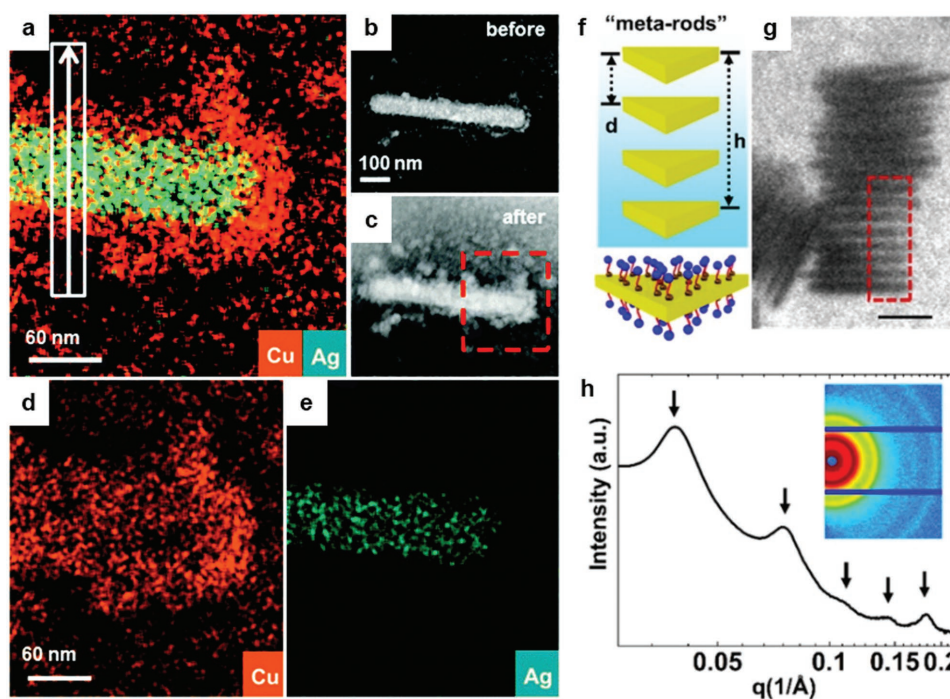
Figure 10. a) EDS elemental map of a Ag–Cu core–shell nanowire in water. b,c) STEM images of the nanowire before (b) and after (c) EDS data acquisition. d,e) Elemental maps of Cu (d) and Ag (e) extracted from panel (a). The elemental map and STEM images clearly show the deposition of Cu nanoparticles around the Ag nanowires. f,g) A schematic diagram (f) and TEM image (g) of self-assembly of Au nanoprisms in 0.15 M phosphate buffer solution at pH 8 (d: d spacing, h: the length of the self-assembled structure) scale bar: 50 nm. h) SAXS spectrum of the self-assembly of Au nanoprisms in 0.15 M phosphate buffer solution at pH 8. The black arrows indicate the peak positions, from which the d spacing of the lamellar structure was calculated. Inset of (h) 2D SAXS image of the same dispersion. a–e) Reproduced with permission.[201] Copyright 2014, Royal Society of Chemistry. f–h) reproduced with permission.[131] Copyright 2016, American Chemical Society

concentration of different radicals. Figure 9c displays the steady-state concentration of different chemical species produced by radiolysis of water.[195] They affect the onset and progress of the nucleation-and-growth behavior of nanoparticles, as well as changing the overall rate of the reaction. Several studies show that switching between reductive and oxidative conditions of the liquid medium can be actively accessed by a careful adjustment of the dose rate.[195,196] Ahmad et al. showed reversible deposition/dissolution of Cu nanoshells on Au nanoparticles in methanol solvents (Figure 9c,d). Under a high dose rate (>6.1 e$^-$ Å^{-2} s^{-1} in their experimental conditions), the generation of e$_{aq}^-$, the reducing radical, is dominant, resulting the growth of Cu nanoshells. In contrast, under a low dose rate (<1.5 e$^-$ Å^{-2} s^{-1} in their experimental conditions), the relative concentration of the oxidizing radicals (CH$_3$OH$^•$) increases, leading to an oxidizing environment that can etch Cu shells.

Another approach to control the radicals produced by the electron beam is introducing radical scavengers into the liquid environment. Because there are different chemical species that have different reactivities toward oxidizing and reducing radicals, selective scavenging of a particular type of radicals is frequently needed. For example, the addition of $^•$OH scavengers can establish a reducing environment free from oxidation reactions by $^•$OH. The study reported by Sutter et al.[89] showed the critical role of alcohol ($^•$OH scavengers) as radical scavengers: two different types of silver-based nanostructures were observed depending on the presence of alcohol. Ag nanoparticles were

transformed into hollow Ag–Pd nanostructures by the galvanic reaction, because the dissolution of Ag (oxidation) and growth of Pd (reduction) take place simultaneously in the absence of alcohol (Figure 3a–c). In the presence of alcohol, however, simple Ag–Pd core–shell structures were formed because alcohol suppresses the oxidation reaction by acting as $^•$OH scavengers. In the other scenario, the addition of halide ions can enhance the oxidation reaction. Halide ions can form secondary radicals (X$_2^{•-}$) which modify the rate of oxidation process via a complexation reaction. In the presence of halide ions, the reduction potential of the metals is decreased, causing an increase of the oxidizing strength of $^•$OH. Hermannsdorfer et al. systematically studied the effect of change in Cl$^-$ concentration on the stability of Au nanoparticles in water (Figure 9b).[197] When the pH is fixed, the addition of Cl$^-$ induced dissolution or coalescence of Au nanoparticles. In addition, faceted nanoparticles were synthesized using this etching process controlled by halide ions.[94] Interestingly, window materials for liquid cells can also act as selective radical scavengers. For example, Wang et al. showed that graphene liquid cells provide more biocompatible environments than Si$_3$N$_4$ liquid cells where biological samples can be sustained under the relatively strong electron-irradiation conditions.[39] A recent study suggested that the use of graphene as a window material or the presence of graphene derivatives in liquid cells can reduce $^•$OH radicals.[95] Recent examples introduced in this section suggest that there are new possibilities to direct electron-beam effects to control

**ADVANCED
SCIENCE NEWS**

www.advancedsciencenews.com

**ADVANCED
MATERIALS**

www.advmat.de

chemical environments of in situ liquid-phase TEM. It is also a consensus that extensive understanding is still needed to quantitatively control the beam effect. More details about current understanding on the electron-beam effects can be found in another recent review paper.[198]

9. Integration with Other Characterization Methods

As we have seen here, liquid-phase TEM is a powerful method for in situ observation of individual nanoparticles. The liquid-phase TEM can be combined with other measurement methods in order to extend understanding of solution chemical reactions with multidimensions, structures in real space and reciprocal space, chemical compositions, and kinetics in single and ensemble nanoparticles.

The readily applicable approaches are analytical methods based on TEM. They include: (i) energy-dispersive X-ray spectroscopy (EDS), (ii) electron energy-loss spectroscopy (EELS), and (iii) ex situ TEM. EDS is widely used to characterize the chemical composition of nanoparticles because its spectrum is element specific.[199,200] Since EDS can be performed in the regular imaging platform of a transmission electron microscope, it is easily combined with liquid-cell TEM. The combination of EDS data and TEM images obtained from the same liquid cell provides detailed understanding of compositional changes of alloys and core–shell nanoparticles.[201,202] Lewis et al. observed Cu deposition onto Ag nanowires and Au nanoparticles in a liquid cell through both high-angle annular dark-field scanning transmission electron microscopy (HADDF-STEM) imaging and EDS elemental mapping (**Figure 10**a–e).[201] EELS can be an alternative to EDS for light elements, but multiple scattering should be considered for liquid samples.[203] However, there is a drawback in that it takes a long time to obtain a high-quality map using EDS or EELS, resulting in poor time resolution. Liquid-cell TEM images are often compared with ex situ TEM images, which are obtained from the sample aliquot during the actual reactions, for two reasons: (i) to obtain structural information with high-resolution,[204] and (ii) to validate that the results from in situ TEM observation are reliable.[131] As discussed in the previous section, the beam effect is mainly induced by the reactive radicals generated by the radiolysis of solvent molecules, and, thus, results with minimized electron-beam perturbation can be obtained from ex situ TEM measurements. Comparing in situ and ex situ TEM, one can identify what extent of in situ observations can be used to understand questions regarding chemical reactions of nanoparticles. Such a combination can be also used to generate redox reaction conditions that cannot be accessed by conventional solution chemistry and investigate behaviors of nanoparticles. For example, during the galvanic replacement between Pd ions and Ag nanoparticles in liquid-cell TEM, radicals generated by the radiolysis of the solvent expedited the homogeneous nucleation of Pd.[89]

Liquid-cell TEM can be complemented with other characterization methods that access ensemble information. Liquid-cell TEM is very useful for single-particle observation, but it takes a very long time and effort to obtain sufficient results to describe ensemble properties. Thus, combining liquid-cell TEM and other in situ techniques,[205] such as SAXS, XRD, and nuclear magnetic resonance (NMR) can help to understand both single-particle properties and ensemble properties.

SAXS is a characterization tool for morphology and the arrangement of nanomaterials. It relies on an elastic scattering signal of X-rays, which is sensitive to the density differences occurring on the nanoscale.[206] The signal of SAXS is determined by the structure factor and form factor. The structure factor is from X-ray diffraction between ordered nanoparticles, and the form factor is related to the shape and size of the nanoparticles. As the particle sizes can be tracked by form-factor analysis, it can be used to investigate the growth processes of nanoparticles in real time.[207–213] Polte et al. studied the size increase of nanoparticles by analyzing the form factor of SAXS spectra during the growth of the Au nanoparticles.[207] Lassemberg et al. found a prenucleate state prior to nanoparticle nucleation by combining form-factor and Porod analysis of SAXS spectra.[214] On the other hand, structure factors depend on the distance and arrangement of many nanoparticles; thus structural information on the self-assembly of nanoparticles has been provided.[208–213] For example, Kim et al. tracked the self-assembly of Au nanoprisms through liquid-cell TEM, and confirmed that the interparticle distance was similar to that measured by SAXS (Figure 10f–h).[131]

Matrix-assisted laser desorption/ionization–time of flight (MALDI-TOF) mass spectrometry is an alternative method to measure the size of nanoparticles.[26–28,31,215] Kim et al. obtained MALDI-TOF mass spectra of ultrasmall-sized iron oxide nanoparticles, smaller than 4 nm, and converted the mass data into a size distribution by using a mass-to-size converting equation.[27] MALDI-TOF mass spectrometry is useful for analyzing the growth process of nanoparticles because it can measure mass information of multiple components in solution growth, including molecules, clusters, and nanoparticles. By using this method, different stages of the growth from the prenucleation state to discrete growth modes in the later stage can be studied. Combining MALDI-TOF MS and liquid-cell TEM would facilitate an understanding of nanoparticle growth with different length scales both at single and ensemble nanoparticle levels.

The growth process and surface structure of nanoparticles can be characterized by NMR. By quantitative analysis of NMR spectra in time, the chemical changes of the precursors during nucleation can be easily traced.[216,217] The binding moiety of surface ligands is also studied by NMR.[218,219] Since the precursors and the surface ligands are not readily visible in TEM images, NMR is expected to be a good complement to liquid-phase TEM studies. Especially, the combination of NMR and the recently developed 3D reconstruction technique of nanoparticles based on liquid-phase TEM can deliver a comprehensive structural understanding of nanoparticles including surface ligands.

10. Conclusions

New characterization technology brings a new understanding of materials chemistry. The recently developed in situ liquid-phase TEM technology enables real-time visualization of the

**ADVANCED
SCIENCE NEWS**

www.advancedsciencenews.com

**ADVANCED
MATERIALS**

www.advmat.de

formation and transformation of nanomaterials. Here, we introduced liquid-phase TEM studies for topics including formation, growth, attachment, transformation, and etching of nanoparticles. We also introduced studies on how the nanomaterial morphology changes under an external bias, including the formation of solid–electrolyte interfaces. Real-time TEM studies have unveiled important mechanistic steps in reactions that could not be studied by conventional methods.

However, studies using liquid-phase TEM are not limited to results introduced here. The formation mechanisms of nanoparticles in different synthetic conditions, including sol–gel, thermal decomposition, coprecipitation, and reverse micelles, await elucidation by liquid-phase TEM. For example, uniformly sized nanoparticles are generally synthesized by thermal decomposition of metal oxide precursors because burst nucleation and separated diffusion-controlled growth can be achieved by this method.[220] However, the formation mechanisms of the thermal decomposition have not been investigated using liquid-phase TEM to date due to the high reaction temperatures, higher than 200 °C.[220–222] In addition, limited literature on nanoparticle behavior modulated by external stimuli, such as temperature and pressure changes and biasing electric potentials, is available.[223]

There is much room for improvement in liquid-cell design and fabrication. Currently, most liquid cells are fabricated by separating two Si_3N_4 windows with spacers and loading the reaction solution between them. However, this method exhibits a very low-resolution due to the unwanted electron-beam scattering of the Si_3N_4 windows, as well as that of the liquid. On the other hand, high-resolution images can be produced with graphene liquid cells; however, control over the thicknesses of the liquid pockets is difficult. Therefore, developing a new liquid cell that can provide high-resolution images with consistent results is needed for reliable experiments. In addition, the new liquid cell should also minimize the interactions between the surface of the liquid cell and the nanoparticles to mimic more realistic reactions.

The development of electron microscopy plays an important role in the advancement of liquid-phase TEM studies. The goal of this new microscopy technique is to obtain high-resolution in situ images using the lowest electron dose with minimal focusing time to minimize the electron-beam effect. It is also desirable to minimize the retention time between loading of the solution sample and TEM imaging. Detectors should also be improved. The smaller the nanoparticle size, the faster it moves and rotates in a liquid. Since TEM images are averaged over exposure time, it is difficult to obtain high-resolution images of nanoparticles when they are small. By significantly reducing the exposure time of the detector with high signal-to-noise ratio, clear images of small nanoparticles in a liquid can be produced.

Liquid-phase TEM shows great potential as an in situ analytic tool in nanoscience, as well as other research areas in engineering and biology. For example, liquid-phase TEM is expected to show structural changes in heterogeneous catalysts during catalytic reactions and deactivation processes. This analytical technique can also be used as an in situ visualization tool to analyze the structure of biomolecules and biological processes.

Conflict of Interest

The authors declare no conflict of interest.

[1] M. H. Nielsen, D. S. Li, H. Z. Zhang, S. Aloni, T. Y. J. Han, C. Frandsen, J. Seto, J. F. Banfield, H. Colfen, J. J. De Yoreo, *Microsc. Microanal.* **2014**, *20*, 425.

[2] F. M. Ross, *Science* **2015**, *350*, aaa9886.

[3] C. M. Wang, H. G. Liao, F. M. Ross, *MRS Bull.* **2015**, *40*, 46.

[4] H. G. Liao, H. M. Zheng, *Ann. Rev. Phys. Chem.* **2016**, *67*, 719.

[5] J. J. De Yoreo, N. A. J. M. Sommerdijk, *Nat. Rev. Mater.* **2016**, *1*, 16035.

[6] L. Marton, *Bull. Cl. Sci., Acad. R. Belg.* **1934**, *20*, 439.

[7] P. Ercius, O. Alaidi, M. J. Rames, G. Ren, *Adv. Mater.* **2015**, *27*, 5638.

[8] M. J. Williamson, R. M. Tromp, P. M. Vereecken, R. Hull, F. M. Ross, *Nat. Mater.* **2003**, *2*, 532.

[9] P. J. M. Smeets, K. R. Cho, R. G. E. Kempen, N. A. J. M. Sommerdijk, J. J. De Yoreo, *Nat. Mater.* **2015**, *14*, 394.

[10] J. Wu, H. Shan, W. Chen, X. Gu, P. Tao, C. Song, W. Shang, T. Deng, *Adv. Mater.* **2016**, *28*, 9686.

[11] C. Wang, Q. Qiao, T. Shokuhfar, R. F. Klie, *Adv. Mater.* **2014**, *26*, 3410.

[12] J. Park, H. Park, P. Ercius, A. F. Pegoraro, C. Xu, J. W. Kim, S. H. Han, D. A. Weitz, *Nano Lett.* **2015**, *15*, 4737.

[13] C. B. Murray, D. J. Norris, M. G. Bawendi, *J. Am. Chem. Soc.* **1993**, *115*, 8706.

[14] A. P. Alivisatos, *Science* **1996**, *271*, 933.

[15] M. V. Kovalenko, L. Manna, A. Cabot, Z. Hens, D. V. Talapin, C. R. Kagan, V. I. Klimov, A. L. Rogach, P. Reiss, D. J. Milliron, P. Guyot-Sionnnest, G. Konstantatos, W. J. Parak, T. Hyeon, B. A. Korgel, C. B. Murray, W. Heiss, *ACS Nano* **2015**, *9*, 1012.

[16] D. V. Talapin, J.-S. Lee, M. V. Kovalenko, E. V. Shevchenko, *Chem. Rev.* **2010**, *110*, 389.

[17] J. Yang, M. K. Choi, D.-H. Kim, T. Hyeon, *Adv. Mater.* **2016**, *28*, 1176.

[18] T. Sugimoto, *Adv. Colloid Interface Sci.* **1987**, *28*, 65.

[19] V. K. Lamer, R. H. Dinegar, *J. Am. Chem. Soc.* **1950**, *72*, 4847.

[20] S. G. Kwon, T. Hyeon, *Small* **2011**, *7*, 2685.

[21] J. Lee, J. Yang, S. G. Kwon, T. Hyeon, *Nat. Rev. Mater.* **2016**, *1*, 16034.

[22] H. Hakkinen, *Chem. Soc. Rev.* **2008**, *37*, 1847.

[23] D. Gebauer, A. Volkel, H. Colfen, *Science* **2008**, *322*, 1819.

[24] J. H. Yu, X. Liu, K. E. Kweon, J. Joo, J. Park, K.-T. Ko, D. W. Lee, S. Shen, K. Tivakornsasithorn, J. S. Son, J.-H. Park, Y.-W. Kim, G. S. Hwang, M. Dobrowolska, J. K. Furdyna, T. Hyeon, *Nat. Mater.* **2010**, *9*, 47.

ADVANCED
SCIENCE NEWS

www.advancedsciencenews.com

ADVANCED
MATERIALS

www.advmat.de

[25] Y.-H. Liu, F. Wang, Y. Wang, P. C. Gibbons, W. E. Buhro, *J. Am. Chem. Soc.* **2011**, *133*, 17005.

[26] J. Yang, R. Fainblat, S. G. Kwon, F. Muckel, J. H. Yu, H. Terlinden, B. H. Kim, D. Iavarone, M. K. Choi, I. Y. Kim, I. Park, H.-K. Hong, J. Lee, J. S. Son, Z. Lee, K. Kang, S.-J. Hwang, G. Bacher, T. Hyeon, *J. Am. Chem. Soc.* **2015**, *137*, 12776.

[27] B. H. Kim, K. Shin, S. G. Kwon, Y. Jang, H.-S. Lee, H. Lee, S. W. Jun, J. Lee, S. Y. Han, Y.-H. Yim, D.-H. Kim, T. Hyeon, *J. Am. Chem. Soc.* **2013**, *135*, 2407.

[28] B. H. Kim, M. J. Hackett, J. Park, T. Hyeon, *Chem. Mater.* **2014**, *26*, 59.

[29] B. M. Cossairt, *Chem. Mater.* **2016**, *28*, 7181.

[30] J. S. Son, J. H. Yu, S. G. Kwon, J. Lee, J. Joo, T. Hyeon, *Adv. Mater.* **2011**, *23*, 3214.

[31] J. Yang, F. Muckel, W. Baek, R. Fainblat, H. Chang, G. Bacher, T. Hyeon, *J. Am. Chem. Soc.* **2017**, *139*, 6761.

[32] A. Radisic, F. M. Ross, P. C. Searson, *J. Phys. Chem. B* **2006**, *110*, 7862.

[33] H. Cho, M. R. Jones, S. C. Nguyen, M. R. Hauwiller, A. Zettl, A. P. Alivisatos, *Nano Lett.* **2017**, *17*, 414.

[34] H. L. L. Xin, H. M. Zheng, *Nano Lett.* **2012**, *12*, 1470.

[35] M. H. Nielsen, J. R. I. Lee, Q. N. Hu, T. Y. J. Han, J. J. De Yoreo, *Faraday Discuss.* **2012**, *159*, 105.

[36] E. A. Ring, N. de Jonge, *Microsc. Microanal.* **2010**, *16*, 622.

[37] M. H. Nielsen, S. Aloni, J. J. De Yoreo, *Science* **2014**, *345*, 1158.

[38] J. M. Yuk, J. Park, P. Ercius, K. Kim, D. J. Hellebusch, M. F. Crommie, J. Y. Lee, A. Zettl, A. P. Alivisatos, *Science* **2012**, *336*, 61.

[39] C. H. Wang, Q. Qiao, T. Shokuhfar, R. F. Klie, *Adv. Mater.* **2014**, *26*, 3410.

[40] J. Zhang, L. Lin, L. Sun, Y. Huang, A. L. Koh, W. Dang, J. Yin, M. Wang, C. Tan, T. Li, Z. Tan, Z. Liu, H. Peng, *Adv. Mater.* **2017**, 1700639.

[41] A.-C. Milazzo, G. Moldovan, J. Lanman, L. Jin, J. C. Bouwer, S. Klienfelder, S. T. Peltier, M. H. Ellisman, A. I. Kirkland, N.-H. Xuong, *Ultramicroscopy* **2010**, *110*, 744.

[42] M. Rossell, M. Watanabe, R. Erni, V. Radmilovic, U. Dahmen, *Microsc. Microanal.* **2009**, *15*, 430.

[43] S. F. Tan, G. Lin, M. Bosman, U. Mirsaidov, C. A. Nijhuis, *ACS Nano* **2016**, *10*, 7689.

[44] D. J. Flannigan, A. H. Zewail, *Acc. Chem. Res.* **2012**, *45*, 1828.

[45] H. M. Zheng, R. K. Smith, Y. W. Jun, C. Kisielowski, U. Dahmen, A. P. Alivisatos, *Science* **2009**, *324*, 1309.

[46] J. E. Evans, K. L. Jungjohann, N. D. Browning, I. Arslan, *Nano Lett.* **2011**, *11*, 2809.

[47] J. Chai, X. Liao, L. R. Giam, C. A. Mirkin, *J. Am. Chem. Soc.* **2012**, *134*, 158.

[48] H. G. Liao, L. K. Cui, S. Whitelam, H. M. Zheng, *Science* **2012**, *336*, 1011.

[49] A. Radisic, P. M. Vereecken, J. B. Hannon, P. C. Searson, F. M. Ross, *Nano Lett.* **2006**, *6*, 238.

[50] D. Li, M. H. Nielsen, J. R. I. Lee, C. Frandsen, J. F. Banfield, J. J. De Yoreo, *Science* **2012**, *336*, 1014.

[51] M. A. van Huis, L. T. Kunneman, K. Overgaag, Q. Xu, G. Pandraud, H. W. Zandbergen, D. Vanmaekelbergh, *Nano Lett.* **2008**, *8*, 3959.

[52] N. D. Loh, S. Sen, M. Bosman, S. F. Tan, J. Zhong, C. A. Nijhuis, P. Král, P. Matsudaira, U. Mirsaidov, *Nat. Chem.* **2017**, *9*, 77.

[53] Z. Y. Li, N. P. Young, M. Di Vece, S. Palomba, R. E. Palmer, A. L. Bleloch, B. C. Curley, R. L. Johnston, J. Jiang, J. Yuan, *Nature* **2008**, *451*, 46.

[54] M. C. Scott, C. C. Chen, M. Mecklenburg, C. Zhu, R. Xu, P. Ercius, U. Dahmen, B. C. Regan, J. W. Miao, *Nature* **2012**, *483*, 444.

[55] S. Van Aert, K. J. Batenburg, M. D. Rossell, R. Erni, G. Van Tendeloo, *Nature* **2011**, *470*, 374.

[56] C. C. Chen, C. Zhu, E. R. White, C. Y. Chiu, M. C. Scott, B. C. Regan, L. D. Marks, Y. Huang, J. W. Miao, *Nature* **2013**, *496*, 74.

[57] M. Azubel, J. Koivisto, S. Malola, D. Bushnell, G. L. Hura, A. L. Koh, H. Tsunoyama, T. Tsukuda, M. Pettersson, H. Hakkinen, R. D. Kornberg, *Science* **2014**, *345*, 909.

[58] Y. Yang, C.-C. Chen, M. C. Scott, C. Ophus, R. Xu, A. Pryor, L. Wu, F. Sun, W. Theis, J. Zhou, M. Eisenbach, P. R. C. Kent, R. F. Sabirianov, H. Zeng, P. Ercius, J. Miao, *Nature* **2017**, *542*, 75.

[59] J. Park, H. Elmlund, P. Ercius, J. M. Yuk, D. T. Limmer, Q. Chen, K. Kim, S. H. Han, D. A. Weitz, A. Zettl, A. P. Alivisatos, *Science* **2015**, *349*, 290.

[60] G. Ouyang, C. X. Wang, G. W. Yang, *Chem. Rev.* **2009**, *109*, 4221.

[61] G. Herrmann, H. Gleiter, G. Baro, *Acta Metall.* **1976**, *24*, 353.

[62] R. L. Penn, J. F. Banfield, *Science* **1998**, *281*, 969.

[63] R. L. Penn, J. F. Banfield, *Am. Mineral.* **1998**, *83*, 1077.

[64] R. L. Penn, J. F. Banfield, *Geochim. Cosmochim. Acta* **1999**, *63*, 1549.

[65] W.-I. Liang, X. Zhang, Y. Zan, M. Pan, C. Czarnik, K. Bustillo, J. Xu, Y.-H. Chu, H. Zheng, *J. Am. Chem. Soc.* **2015**, *137*, 14850.

[66] K.-Y. Niu, M. Liu, K. A. Persson, Y. Han, H. Zheng, *ACS Nano* **2016**, *10*, 6235.

[67] K. L. Jungjohann, S. Bliznakov, P. W. Sutter, E. A. Stach, E. A. Sutter, *Nano Lett.* **2013**, *13*, 2964.

[68] H.-W. Liang, S. Liu, S.-H. Yu, *Adv. Mater.* **2010**, *22*, 3925.

[69] S. Gupta, S. V. Kershaw, A. L. Rogach, *Adv. Mater.* **2013**, *25*, 6923.

[70] L. Yu, H. Hu, H. B. Wu, X. W. Lou, *Adv. Mater.* **2017**, *29*, 1604563.

[71] Y. Sun, Y. Xia, *Science* **2002**, *298*, 2176.

[72] Y. Yin, R. M. Rioux, C. K. Erdonmez, S. Hughes, G. A. Somorjai, A. P. Alivisatos, *Science* **2004**, *304*, 711.

[73] B. Wiley, T. Herricks, Y. Sun, Y. Xia, *Nano Lett.* **2004**, *4*, 1733.

[74] Y. Xia, Y. Xiong, B. Lim, S. E. Skrabalak, *Angew. Chem.* **2009**, *121*, 62; *Angew. Chem., Int. Ed.* **2009**, *48*, 60.

[75] A. Cabot, M. Ibáñez, P. Guardia, A. P. Alivisatos, *J. Am. Chem. Soc.* **2009**, *131*, 11326.

[76] S. Peng, S. Sun, *Angew. Chem.* **2007**, *119*, 4233; *Angew. Chem., Int. Ed.* **2007**, *46*, 4155.

[77] E. V. Shevchenko, M. I. Bodnarchuk, M. V. Kovalenko, D. V. Talapin, R. K. Smith, S. Aloni, W. Heiss, A. P. Alivisatos, *Adv. Mater.* **2008**, *20*, 4323.

[78] Q. Wang, S. Chen, F. Shi, K. Chen, Y. Nie, Y. Wang, R. Wu, J. Li, Y. Zhang, W. Ding, Y. Li, L. Li, Z. Wei, *Adv. Mater.* **2016**, *28*, 10673.

[79] M. H. Oh, T. Yu, S.-H. Yu, B. Lim, K.-T. Ko, M.-G. Willinger, D.-H. Seo, B. H. Kim, M. G. Cho, J.-H. Park, K. Kang, Y.-E. Sung, N. Pinna, T. Hyeon, *Science* **2013**, *340*, 964.

[80] K. Y. Niu, J. Park, H. M. Zheng, A. P. Aivisatos, *Nano Lett.* **2013**, *13*, 5715.

[81] X. Xia, Y. Wang, A. Ruditskiy, Y. Xia, *Adv. Mater.* **2013**, *25*, 6313.

[82] X. Liu, D. Astruc, *Adv. Mater.* **2017**, *29*, 1605305.

[83] E. González, J. Arbiol, V. F. Puntes, *Science* **2011**, *334*, 1377.

[84] Y. Sun, Y. Xia, *J. Am. Chem. Soc.* **2004**, *126*, 3892.

[85] S. E. Skrabalak, J. Chen, Y. Sun, X. Lu, L. Au, C. M. Cobley, Y. Xia, *Acc. Chem. Res.* **2008**, *41*, 1587.

[86] G. S. Métraux, Y. C. Cao, R. Jin, C. A. Mirkin, *Nano Lett.* **2003**, *3*, 519.

[87] Z. Peng, H. You, J. Wu, H. Yang, *Nano Lett.* **2010**, *10*, 1492.

[88] J. E. Macdonald, M. Bar Sadan, L. Houben, I. Popov, U. Banin, *Nat. Mater.* **2010**, *9*, 810.

[89] E. Sutter, K. Jungjohann, S. Bliznakov, A. Courty, E. Maisonhaute, S. Tenney, P. Sutter, *Nat. Commun.* **2014**, *5*, 4946.

[90] C. Wang, M. Chi, D. Li, D. Strmcnik, D. van der Vliet, G. Wang, V. Komanicky, K.-C. Chang, A. P. Paulikas, D. Tripkovic, J. Pearson, K. L. More, N. M. Markovic, V. R. Stamenkovic, *J. Am. Chem. Soc.* **2011**, *133*, 14396.

[91] V. R. Stamenkovic, B. S. Mun, K. J. J. Mayrhofer, P. N. Ross, N. M. Markovic, *J. Am. Chem. Soc.* **2006**, *128*, 8813.

[92] K. An, S. G. Kwon, M. Park, H. B. Na, S.-I. Baik, J. H. Yu, D. Kim, J. S. Son, Y. W. Kim, I. C. Song, W. K. Moon, H. M. Park, T. Hyeon, *Nano Lett.* **2008**, *8*, 4252.

[93] W.-S. Cho, R. Duffin, S. E. Howie, C. J. Scotton, W. A. Wallace, W. MacNee, M. Bradley, I. L. Megson, K. Donaldson, *Part. Fibre Toxicol.* **2011**, *8*, 27.

[94] Y. Jiang, G. Zhu, F. Lin, H. Zhang, C. Jin, J. Yuan, D. Yang, Z. Zhang, *Nano Lett.* **2014**, *14*, 3761.

[95] X. Ye, M. R. Jones, L. B. Frechette, Q. Chen, A. S. Powers, P. Ercius, G. Dunn, G. M. Rotskoff, S. C. Nguyen, V. P. Adiga, A. Zettl, E. Rabani, P. L. Geissler, A. P. Alivisatos, *Science* **2016**, *354*, 874.

[96] W. Cui, Z. Shen, J. Yang, S. Wu, *Appl. Therm. Eng.* **2015**, *76*, 261.

[97] H. Zheng, S. A. Claridge, A. M. Minor, A. P. Alivisatos, U. Dahmen, *Nano Lett.* **2009**, *9*, 2460.

[98] N. de Jonge, N. Poirier-Demers, H. Demers, D. B. Peckys, D. Drouin, *Ultramicroscopy* **2010**, *110*, 1114.

[99] C. Mueller, M. Harb, J. R. Dwyer, R. J. D. Miller, *J. Phys. Chem. Lett.* **2013**, *4*, 2339.

[100] A. Einstein, *Ann. Phys.* **1905**, *322*, 549.

[101] A. Verch, M. Pfaff, N. de Jonge, *Langmuir* **2015**, *31*, 6956.

[102] J. Lu, Z. Aabdin, N. D. Loh, D. Bhattacharya, U. Mirsaidov, *Nano Lett.* **2014**, *14*, 2111.

[103] S. W. Chee, Z. Baraissov, N. D. Loh, P. T. Matsudaira, U. Mirsaidov, *J. Phys. Chem. C* **2016**, *120*, 20462.

[104] W. C. Lee, B. H. Kim, S. Choi, S. Takeuchi, J. Park, *J. Phys. Chem. Lett.* **2017**, *8*, 647.

[105] Y. Liu, X.-M. Lin, Y. Sun, T. Rajh, *J. Am. Chem. Soc.* **2013**, *135*, 3764.

[106] E. R. White, M. Mecklenburg, B. Shevitski, S. B. Singer, B. C. Regan, *Langmuir* **2012**, *28*, 3695.

[107] H. Zheng, *Nanoscale* **2013**, *5*, 4070.

[108] H. Zheng, U. M. Mirsaidov, L.-W. Wang, P. Matsudaira, *Nano Lett.* **2012**, *12*, 5644.

[109] M. W. P. van de Put, C. C. M. C. Carcouët, P. H. H. Bomans, H. Friedrich, N. de Jonge, N. A. J. M. Sommerdijk, *Small* **2015**, *11*, 585.

[110] X. Fu, B. Chen, J. Tang, M. T. Hassan, A. H. Zewail, *Science* **2017**, *355*, 494.

[111] H. G. Liao, K. Niu, H. Zheng, *Chem. Commun.* **2013**, *49*, 11720.

[112] Q. Chen, H. Cho, K. Manthiram, M. Yoshida, X. Ye, A. P. Alivisatos, *ACS Cent. Sci.* **2015**, *1*, 33.

[113] Q. Chen, J. M. Smith, J. Park, K. Kim, D. Ho, H. I. Rasool, A. Zettl, A. P. Alivisatos, *Nano Lett.* **2013**, *13*, 4556.

[114] D. Ling, W. Park, S.-j. Park, Y. Lu, K. S. Kim, M. J. Hackett, B. H. Kim, Y. Yim, Y. S. Jeon, K. Na, T. Hyeon, *J. Am. Chem. Soc.* **2014**, *136*, 5647.

[115] H. S. Choi, W. Liu, P. Misra, E. Tanaka, J. P. Zimmer, B. I. Ipe, M. G. Bawendi, J. V. Frangioni, *Nat. Biotechnol.* **2007**, *25*, 1165.

[116] E. S. Pohlmann, K. Patel, S. Guo, M. J. Dukes, Z. Sheng, D. F. Kelly, *Nano Lett.* **2015**, *15*, 2329.

[117] S. Sun, *Adv. Mater.* **2006**, *18*, 393.

[118] M.-C. Daniel, D. Astruc, *Chem. Rev.* **2004**, *104*, 293.

[119] J. Zhang, Y. Li, X. Zhang, B. Yang, *Adv. Mater.* **2010**, *22*, 4249.

[120] J. F. Galisteo-López, M. Ibisate, R. Sapienza, L. S. Froufe-Pérez, Á. Blanco, C. López, *Adv. Mater.* **2011**, *23*, 30.

[121] L. Vigderman, B. P. Khanal, E. R. Zubarev, *Adv. Mater.* **2012**, *24*, 4811.

[122] J. J. Geuchies, C. van Overbeek, W. H. Evers, B. Goris, A. de Backer, A. P. Gantapara, F. T. Rabouw, J. Hilhorst, J. L. Peters, O. Konovalov, A. V. Petukhov, M. Dijkstra, L. D. A. Siebbeles, S. van Aert, S. Bals, D. Vanmaekelbergh, *Nat. Mater.* **2016**, *15*, 1248.

[123] B. A. Legg, M. Zhu, L. R. Comolli, B. Gilbert, J. F. Banfield, *Environ. Sci. Technol.* **2014**, *48*, 13703.

[124] S. Narayanan, J. Wang, X.-M. Lin, *Phys. Rev. Lett.* **2004**, *93*, 135503.

[125] J. Park, H. Zheng, W. C. Lee, P. L. Geissler, E. Rabani, A. P. Alivisatos, *ACS Nano* **2012**, *6*, 2078.

[126] A. S. Powers, H.-G. Liao, S. N. Raja, N. D. Bronstein, A. P. Alivisatos, H. Zheng, *Nano Lett.* **2017**, *17*, 15.

[127] J. Liu, Z. Wang, A. Sheng, F. Liu, F. Qin, Z. L. Wang, *Environ. Sci. Technol.* **2016**, *50*, 5606.

[128] Y. Lin, H. Skaff, T. Emrick, A. D. Dinsmore, T. P. Russell, *Science* **2003**, *299*, 226.

[129] G. Lin, X. Zhu, U. Anand, Q. Liu, J. Lu, Z. Aabdin, H. Su, U. Mirsaidov, *Nano Lett.* **2016**, *16*, 1092.

[130] E. Sutter, P. Sutter, A. V. Tkachenko, R. Krahne, J. de Graaf, M. Arciniegas, L. Manna, *Nat. Commun.* **2016**, *7*.

[131] J. Kim, M. R. Jones, Z. Ou, Q. Chen, *ACS Nano* **2016**, *10*, 9801.

[132] K. Y. Niu, H. G. Liao, H. M. Zheng, *Microsc. Microanal.* **2014**, *20*, 416.

[133] C. Lu, Z. Tang, *Adv. Mater.* **2016**, *28*, 1096.

[134] J. H. Yu, J. Joo, H. M. Park, S.-I. Baik, Y. W. Kim, S. C. Kim, T. Hyeon, *J. Am. Chem. Soc.* **2005**, *127*, 5662.

[135] S. Shaw, L. Cademartiri, *Adv. Mater.* **2013**, *25*, 4829.

[136] N. P. Dasgupta, J. Sun, C. Liu, S. Brittman, S. C. Andrews, J. Lim, H. Gao, R. Yan, P. Yang, *Adv. Mater.* **2014**, *26*, 2137.

[137] C. S. S. Sandeep, J. M. Azpiroz, W. H. Evers, S. C. Boehme, I. Moreels, S. Kinge, L. D. A. Siebbeles, I. Infante, A. J. Houtepen, *ACS Nano* **2014**, *8*, 11499.

[138] Z. Quan, D. Wu, J. Zhu, W. H. Evers, J. M. Boncella, L. D. A. Siebbeles, Z. Wang, A. Navrotsky, H. Xu, *Proc. Natl. Acad. Sci.* **2014**, *111*, 9054.

[139] Z. Yang, E. Yassitepe, O. Voznyy, A. Janmohamed, X. Lan, L. Levina, R. Comin, E. H. Sargent, *J. Am. Chem. Soc.* **2015**, *137*, 14869.

[140] W. J. Baumgardner, K. Whitham, T. Hanrath, *Nano Lett.* **2013**, *13*, 3225.

[141] W. H. Evers, B. Goris, S. Bals, M. Casavola, J. de Graaf, R. van Roij, M. Dijkstra, D. Vanmaekelbergh, *Nano Lett.* **2013**, *13*, 2317.

[142] M. P. Boneschanscher, W. H. Evers, J. J. Geuchies, T. Altantzis, B. Goris, F. T. Rabouw, S. A. P. van Rossum, H. S. J. van der Zant, L. D. A. Siebbeles, G. Van Tendeloo, I. Swart, J. Hilhorst, A. V. Petukhov, S. Bals, D. Vanmaekelbergh, *Science* **2014**, *344*, 1377.

[143] K. Whitham, J. Yang, B. H. Savitzky, L. F. Kourkoutis, F. Wise, T. Hanrath, *Nat. Mater.* **2016**, *15*, 557.

[144] S. J. Oh, Z. Wang, N. E. Berry, J.-H. Choi, T. Zhao, E. A. Gaulding, T. Paik, Y. Lai, C. B. Murray, C. R. Kagan, *Nano Lett.* **2014**, *14*, 6210.

[145] U. Anand, J. Lu, D. Loh, Z. Aabdin, U. Mirsaidov, *Nano Lett.* **2016**, *16*, 786.

[146] Z. Aabdin, J. Lu, X. Zhu, U. Anand, N. D. Loh, H. Su, U. Mirsaidov, *Nano Lett.* **2014**, *14*, 6639.

[147] G. Lin, S. W. Chee, S. Raj, P. Král, U. Mirsaidov, *ACS Nano* **2016**, *10*, 7443.

[148] Z.-R. Chang, H.-J. Lv, H.-W. Tang, H.-J. Li, X.-Z. Yuan, H. Wang, *Electrochim. Acta* **2009**, *54*, 4595.

[149] Y. Talyosef, B. Markovsky, G. Salitra, D. Aurbach, H. J. Kim, S. Choi, *J. Power Sources* **2005**, *146*, 664.

[150] M. S. Whittingham, *Chem. Rev.* **2004**, *104*, 4271.

[151] D. Chao, X. Xia, J. Liu, Z. Fan, C. F. Ng, J. Lin, H. Zhang, Z. X. Shen, H. J. Fan, *Adv. Mater.* **2014**, *26*, 5794.

[152] X. Rui, W. Sun, C. Wu, Y. Yu, Q. Yan, *Adv. Mater.* **2015**, *27*, 6670.

[153] G. Zhou, S. Pei, L. Li, D. W. Wang, S. Wang, K. Huang, L. C. Yin, F. Li, H. M. Cheng, *Adv. Mater.* **2014**, *26*, 625.

[154] A. R. Kamali, D. J. Fray, *J. New Mater. Electrochem. Syst.* **2010**, *13*, 147.

[155] Y. Tang, L. Yang, Z. Qiu, J. Huang, *J. Mater. Chem.* **2009**, *19*, 5980.

[156] P. Verma, P. Maire, P. Novák, *Electrochim. Acta* **2010**, *55*, 6332.

[157] S. Yuan, X. L. Huang, D. L. Ma, H. G. Wang, F. Z. Meng, X. B. Zhang, *Adv. Mater.* **2014**, *26*, 2273.

[158] X. Zhou, L. J. Wan, Y. G. Guo, *Adv. Mater.* **2013**, *25*, 2152.

[159] J. Chen, L. Xu, W. Li, X. Gou, *Adv. Mater.* **2005**, *5*, 582.

[160] D. Aurbach, Y. Talyosef, B. Markovsky, E. Markevich, E. Zinigrad, L. Asraf, J. S. Gnanaraj, H.-J. Kim, *Electrochim. Acta* **2004**, *50*, 247.

[161] J. Li, C. Ma, M. Chi, C. Liang, N. J. Dudney, *Adv. Energy Mater.* **2015**, *5*, 1401408.

[162] Y. Liu, D. Lin, P. Y. Yuen, K. Liu, J. Xie, R. H. Dauskardt, Y. Cui, *Adv. Mater.* **2017**, *29*, 1605531.

[163] M.-T. F. Rodrigues, K. Kalaga, H. Gullapalli, G. Babu, A. L. M. Reddy, P. M. Ajayan, *Adv. Energy Mater.* **2016**, *6*, 1600218.

[164] C. Zuo, S. Zha, M. Liu, M. Hatano, M. Uchiyama, *Adv. Mater.* **2006**, *18*, 3318.

[165] S. W. Tao, J. T. S. Irvine, *Adv. Mater.* **2006**, *18*, 1581.

[166] L. F. Cui, Y. Yang, C. M. Hsu, Y. Cui, *Nano Lett.* **2009**, *9*, 3370.

[167] W. Y. Li, L. N. Xu, J. Chen, *Adv. Funct. Mater.* **2005**, *15*, 851.

[168] Y. Li, B. Tan, Y. Wu, *Nano Lett.* **2008**, *8*, 265.

[169] J. Liu, F. Liu, K. Gao, J. Wu, D. Xue, *J. Mater. Chem.* **2009**, *19*, 6073.

[170] S. L. P. Poizot, S. Grugeon, L. Dupont, J.-M. Tarascon, *Nature* **2000**, *407*, 496.

[171] M. V. Reddy, G. V. Subba Rao, B. V. Chowdari, *Chem. Rev.* **2013**, *113*, 5364.

[172] H. L. Wang, L. F. Cui, Y. A. Yang, H. S. Casalongue, J. T. Robinson, Y. Y. Liang, Y. Cui, H. J. Dai, *J. Am. Chem. Soc.* **2010**, *132*, 13978.

[173] E. Yoo, J. Kim, E. Hosono, H. Zhou, T. Kudo, I. Honma, *Nano Lett.* **2008**, *8*, 2277.

[174] L.-S. Zhang, L.-Y. Jiang, H.-J. Yan, W. D. Wang, W. Wang, W.-G. Song, Y.-G. Guo, L.-J. Wan, *J. Mater. Chem.* **2010**, *20*, 5462.

[175] S.-K. Jung, H. Gwon, J. Hong, K.-Y. Park, D.-H. Seo, H. Kim, J. Hyun, W. Yang, K. Kang, *Adv. Energy Mater.* **2014**, *4*, 1300787.

[176] F. S. Li, Y. S. Wu, J. Chou, M. Winter, N. L. Wu, *Adv. Mater.* **2015**, *27*, 130.

[177] J. Y. Huang, L. Zhong, C. M. Wang, J. P. Sullivan, W. Xu, L. Q. Zhang, S. X. Mao, N. S. Hudak, X. H. Liu, A. Subramanian, H. Y. Fan, L. A. Qi, A. Kushima, J. Li, *Science* **2010**, *330*, 1515.

[178] X. H. Liu, J. W. Wang, Y. Liu, H. Zheng, A. Kushima, S. Huang, T. Zhu, S. X. Mao, J. Li, S. Zhang, W. Lu, J. M. Tour, J. Y. Huang, *Carbon* **2012**, *50*, 3836.

[179] X. H. Liu, H. Zheng, L. Zhong, S. Huang, K. Karki, L. Q. Zhang, Y. Liu, A. Kushima, W. T. Liang, J. W. Wang, J. H. Cho, E. Epstein, S. A. Dayeh, S. T. Picraux, T. Zhu, J. Li, J. P. Sullivan, J. Cumings, C. Wang, S. X. Mao, Z. Z. Ye, S. Zhang, J. Y. Huang, *Nano Lett.* **2011**, *11*, 3312.

[180] C. M. Wang, W. Xu, J. Liu, D. W. Choi, B. Arey, L. V. Saraf, J. G. Zhang, Z. G. Yang, S. Thevuthasan, D. R. Baer, N. Salmon, *J. Mater. Res.* **2011**, *25*, 1541.

[181] R. R. Unocic, R. L. Sacci, G. M. Brown, G. M. Veith, N. J. Dudney, K. L. More, F. S. Walden II, D. S. Gardiner, J. Damiano, D. P. Nackashi, *Microsc. Microanal.* **2014**, *20*, 452.

[182] Z. Zeng, W. I. Liang, H. G. Liao, H. L. Xin, Y. H. Chu, H. Zheng, *Nano Lett.* **2014**, *14*, 1745.

[183] M. Gu, L. R. Parent, B. L. Mehdi, R. R. Unocic, M. T. McDowell, R. L. Sacci, W. Xu, J. G. Connell, P. Xu, P. Abellan, X. Chen, Y. Zhang, D. E. Perea, J. E. Evans, L. J. Lauhon, J.-G. Zhang, J. Liu, N. D. Browning, Y. Cui, I. Arslan, C.-M. Wang, *Nano Lett.* **2013**, *13*, 6106.

[184] Z. Zeng, W.-I. Liang, Y.-H. Chu, H. Zheng, *Faraday Discuss.* **2014**, *176*, 95.

[185] Z. Zeng, X. Zhang, K. Bustillo, K. Niu, C. Gammer, J. Xu, H. Zheng, *Nano Lett.* **2015**, *15*, 5214.

[186] Z. Zeng, W. Zheng, H. Zheng, *Acc. Chem. Res.* **2017**, *50*, 1808.

[187] P. Abellan, B. L. Mehdi, L. R. Parent, M. Gu, C. Park, W. Xu, Y. Zhang, I. Arslan, J.-G. Zhang, C.-M. Wang, J. E. Evans, N. D. Browning, *Nano Lett.* **2014**, *14*, 1293.

[188] M. E. Holtz, Y. Yu, D. Gunceler, J. Gao, R. Sundararaman, K. A. Schwarz, T. A. Arias, H. D. Abruña, D. A. Muller, *Nano Lett.* **2014**, *14*, 1453.

[189] R. L. Sacci, N. J. Dudney, K. L. More, L. R. Parent, I. Arslan, N. D. Browning, R. R. Unocic, *Chem. Commun.* **2014**, *50*, 2104.

[190] R. L. Sacci, J. M. Black, N. Balke, N. J. Dudney, K. L. More, R. R. Unocic, *Nano Lett.* **2015**, *15*, 2011.

[191] B. L. Mehdi, J. Qian, E. Nasybulin, C. Park, D. A. Welch, R. Faller, H. Mehta, W. A. Henderson, W. Xu, C. M. Wang, J. E. Evans, J. Liu, J. G. Zhang, K. T. Mueller, N. D. Browning, *Nano Lett.* **2015**, *15*, 2168.

[192] R. R. Unocic, X.-G. Sun, R. L. Sacci, L. A. Adamczyk, D. H. Alsem, S. Dai, N. J. Dudney, K. L. More, *Microsc. Microanal.* **2014**, *20*, 1029.

[193] A. J. Leenheer, K. L. Jungjohann, K. R. Zavadil, J. P. Sullivan, C. T. Harris, *ACS Nano* **2015**, *9*, 4379.

[194] A. O. Allen, *The Radiation Chemistry of Water and Aqueous Solutions*, Van Nostrand, Princeton, NJ **1961**.

[195] N. M. Schneider, M. M. Norton, B. J. Mendel, J. M. Grogan, F. M. Ross, H. H. Bau, *J. Phys. Chem. C* **2014**, *118*, 22373.

[196] N. Ahmad, G. Wang, J. Nelayah, C. Ricolleau, D. Alloyeau, *J. Microsc.* **2017**, https://doi.org/10.1111/jmi.12568.

[197] J. Hermannsdorfer, N. de Jonge, A. Verch, *Chem. Commun.* **2015**, *51*, 16393.

[198] T. J. Woehl, P. Abellan, *J. Microsc.* **2017**, *265*, 135.

[199] A. Singh, A. Singh, J. Ciston, K. Bustillo, D. Nordlund, D. J. Milliron, *J. Am. Chem. Soc.* **2015**, *137*, 6464.

[200] D. Zhang, A. B. Wong, Y. Yu, S. Brittman, J. Sun, A. Fu, B. Beberwyck, A. P. Alivisatos, P. Yang, *J. Am. Chem. Soc.* **2014**, *136*, 17430.

[201] E. A. Lewis, S. J. Haigh, T. J. A. Slater, Z. He, M. A. Kulzick, M. G. Burke, N. J. Zaluzec, *Chem. Commun.* **2014**, *50*, 10019.

[202] N. J. Zaluzec, M. G. Burke, S. J. Haigh, M. A. Kulzick, *Microsc. Microanal.* **2014**, *20*, 323.

[203] M. E. Holtz, Y. Yu, J. Gao, H. D. Abruña, D. A. Muller, *Microsc. Microanal.* **2013**, *19*, 1027.

[204] Y. Yuan, S. M. Wood, K. He, W. Yao, D. Tompsett, J. Lu, A. Nie, M. S. Islam, R. Shahbazian-Yassar, *ACS Nano* **2016**, *10*, 539.

[205] Y. Yang, X. Liu, Z. Dai, F. Yuan, Y. Bando, D. Golberg, X. Wang, *Adv. Mater.* **2017**, *29*, 1606922.

[206] T. Li, A. J. Senesi, B. Lee, *Chem. Rev.* **2016**, *116*, 11128.

[207] J. Polte, T. T. Ahner, F. Delissen, S. Sokolov, F. Emmerling, A. F. Thünemann, R. Kraehnert, *J. Am. Chem. Soc.* **2010**, *132*, 1296.

[208] H. Koerner, R. I. MacCuspie, K. Park, R. A. Vaia, *Chem. Mater.* **2012**, *24*, 981.

[209] F. Pietra, F. T. Rabouw, W. H. Evers, D. V. Byelov, A. V. Petukhov, C. de Mello Donegá, D. Vanmaekelbergh, *Nano Lett.* **2012**, *12*, 5515.

[210] E. Josten, E. Wetterskog, A. Glavic, P. Boesecke, A. Feoktystov, E. Brauweiler-Reuters, U. Rücker, G. Salazar-Alvarez, T. Brückel, L. Bergström, *Sci. Rep.* **2017**, *7*, 2802.

[211] Z. Jiang, X.-M. Lin, M. Sprung, S. Narayanan, J. Wang, *Nano Lett.* **2010**, *10*, 799.

[212] M. C. Weidman, D.-M. Smilgies, W. A. Tisdale, *Nat. Mater.* **2016**, *15*, 775.

[213] P. Siffalovic, E. Majkova, L. Chitu, M. Jergel, S. Luby, A. Satka, S. V. Roth, *Phys. Rev. B* **2007**, *76*, 195432.

[214] A. Lassenberger, T. A. Grünewald, P. D. J. van Oostrum, H. Rennhofer, H. Amenitsch, R. Zirbs, H. C. Lichtenegger, E. Reimhult, *Chem. Mater.* **2017**, *29*, 4511.

[215] F. Muckel, J. Yang, S. Lorenz, W. Baek, H. Chang, T. Hyeon, G. Bacher, R. Fainblat, *ACS Nano* **2016**, *10*, 7135.

[216] V. N. Richards, N. P. Rath, W. E. Buhro, *Chem. Mater.* **2010**, *22*, 3556.

**ADVANCED
SCIENCE NEWS**

www.advancedsciencenews.com

**ADVANCED
MATERIALS**

www.advmat.de

[217] J. S. Owen, E. M. Chan, H. Liu, A. P. Alivisatos, *J. Am. Chem. Soc.* **2010**, *132*, 18206.

[218] B. Fritzinger, I. Moreels, P. Lommens, R. Koole, Z. Hens, J. C. Martins, *J. Am. Chem. Soc.* **2009**, *131*, 3024.

[219] J. De Roo, I. Van Driessche, J. C. Martins, Z. Hens, *Nat. Mater.* **2016**, *15*, 517.

[220] S. G. Kwon, Y. Piao, J. Park, S. Angappane, Y. Jo, N.-M. Hwang, J.-G. Park, T. Hyeon, *J. Am. Chem. Soc.* **2007**, *129*, 12571.

[221] J. Park, J. Joo, S. G. Kwon, Y. Jang, T. Hyeon, *Angew. Chem.* **2007**, *119*, 4714; *Angew. Chem., Int. Ed.* **2007**, *46*, 4630.

[222] B. H. Kim, N. Lee, H. Kim, K. An, Y. I. Park, Y. Choi, K. Shin, Y. Lee, S. G. Kwon, H. B. Na, J.-G. Park, T.-Y. Ahn, Y.-W. Kim, W. K. Moon, S. H. Choi, T. Hyeon, *J. Am. Chem. Soc.* **2011**, *133*, 12624.

[223] G.-Z. Zhu, S. Prabhudev, J. Yang, C. M. Gabardo, G. A. Botton, L. Soleymani, *J. Phys. Chem. C* **2014**, *118*, 22111.

1703316 (20 of 20)